31. THE INTRINSIC MAGNETIC FIELD AND SOLAR-WIND INTERACTION OF MARS

J. G. LUHMANN, C. T. RUSSELL
University of California, Los Angeles

L. H. BRACE
University of Michigan

and
O. L. VAISBERG
Space Research Institute, Moscow

Plasma and field measurements on various spacecraft have demonstrated that Mars has an intrinsic dipole magnetic field that is no more than $\sim 10^{-4}$ times as strong as that of the Earth. This difference is attributed to the weakness or absence of dynamo activity in the Martian core. An important consequence of the weak intrinsic field is a Venus-like interaction between the solar wind and the atmosphere. It has been found that this interaction leads to losses of Martian atmosphere constituents that are important for the atmosphere's evolution.

INTRODUCTION

A. Intrinsic Planetary Magnetic Fields

It has been known for over 500 yr that the Earth possesses an intrinsic magnetic field, approximately dipolar, like that of a bar magnet (Gilbert 1600). This field is generated by a dynamo produced by convection in the electrically conducting, rotating, molten core (Gubbins 1974). In the last century astronomers have discovered that the Sun as well as stars in general also generate their own magnetic fields. One of the first discoveries of radio astronomy was the existence of emissions from Jupiter (Burke and Franklin 1955) which enabled astronomers to discover and remotely measure the magnetic field of Jupiter. Since the advent of interplanetary space flight, we have had the opportunity to measure directly the magnetic fields at Jupiter and many of the other planets. Some planets, like Jupiter, Saturn and Uranus, have intrinsic magnetic moments much larger than that of the Earth. Others, like Mercury, Venus and Mars, possess much weaker magnetic moments. The reasons for these differences, which have to do with the properties of the interiors of these planets and the nature of their dynamos, are subjects of continuing study.

Of particular interest are the differences between the fields of the terrestrial planets Earth, Venus and Mars. The history and current state of the interiors of our two neighboring planets appear to be considerably different from those of Earth. Venus is distinguished by the fact that it is a slower rotator, (243-day period) while it is similar in size to Earth (6050-km radius vs Earth's 6370 km). Mars is distinguished by its smaller size (1 $R_M \approx$ 3390-km radius) while it rotates at about the same rate as Earth (~24.6-hr period). The question of how these differences translate into different internal properties has been under investigation, but the uncertainty in the results of these studies is compounded by the lack of seismic data from Venus and Mars. In any event, it is clear that the weak magnetic field of Mars would present a puzzle if size and rotation rate were the only dominant factors controlling planetary dynamos because Mars is not unlike Earth in those respects.

B. Solar-Wind Interactions

When a planetary magnetic field is weak, like that of Mars, the solar wind strongly distorts its configuration. For this reason, it is difficult to infer the strength of the intrinsic magnetic field from observations without understanding the solar-wind interaction.

The expanding magnetized plasma atmosphere of the Sun, the solar wind, produces a quite different environment when it interacts directly with a planetary atmosphere than when it interacts with a planetary magnetic field. Nevertheless, there are a few elements common to both. These common elements, which are illustrated in Fig. 1, include a bow shock standing in the solar wind upstream of the "obstacle" that slows and deflects the flow, and a region between the shock and the obstacle, known as the magnetosheath, in which the solar-wind plasma and magnetic field are compressed. If the interplanetary magnetic field is oriented at a substantial angle to the upstream flow, the field appears to drape around the obstacle. The differences between the atmospheric and magnetic field obstacle, which are more numerous, are schematically illustrated in Fig. 2.

Figure 2 shows the basic features of the interactions of several kinds of planetary obstacles with the solar wind. In the case of a dipole field, the

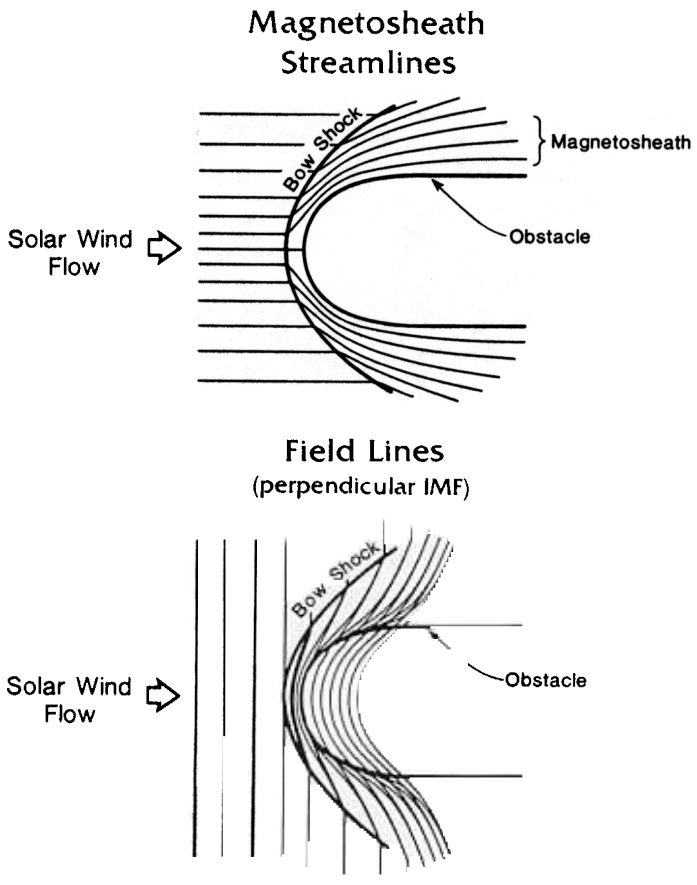

Fig. 1. Illustration of the solar-wind plasma flow (top) and draped interplanetary magnetic field (bottom) in a planetary magnetosheath.

obstacle is defined by the boundary between the shocked solar wind and the region dominated by the dipole field where the component of the solar-wind pressure normal to the surface equals the magnetic pressure of the internal field (Fig. 2a). This boundary is called a magnetopause. In the case where the atmosphere of a weakly magnetized planet is responsible for the analogous boundary, an ionopause forms where the pressure of the ionospheric plasma balances the incident solar-wind pressure (Fig. 2b). The latter is transformed to magnetic pressure above the ionopause where it forms an effective magnetic barrier between the solar-wind plasma and the relatively cold ionospheric plasma (although ionospheric ions are still produced within the barrier). If the solar-wind pressure exceeds the ionospheric pressure, the location of the ionopause can be modified by a magnetic field that is induced

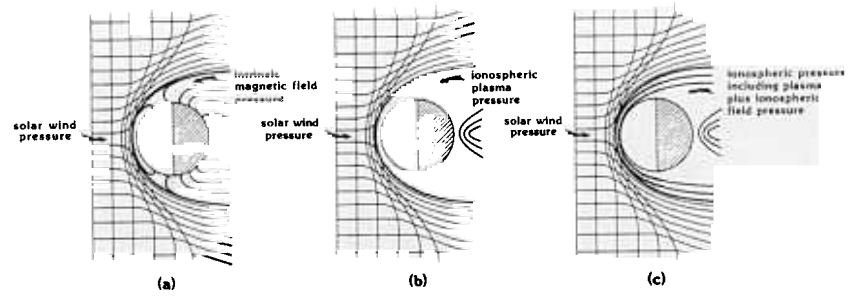

Fig. 2. Schematic sketch showing three types of planetary obstacles to the solar wind: (a) a magnetospheric obstacle where the incident solar-wind dynamic pressure is balanced by the pressure of the internal dipole field; (b) an atmospheric or ionospheric obstacle where the thermal pressure of the ionospheric plasma balances the solar-wind pressure; and (c) an ionospheric obstacle whose internal pressure is supplemented by an ionospheric magnetic field of interplanetary origin.

in the ionosphere by the solar-wind interaction (Fig. 2c). Since the scale length of gradients of pressure for planetary magnetic fields is the order of a planetary radius, while the scale length of a planetary atmosphere or ionosphere is only 10s to 100s of km, we expect the obstacle associated with a weakly magnetized planet to be much closer to the planet and much less compressible than the obstacle created by a magnetized planet. If an intrinsic magnetic field of marginal strength is present, the boundary is likely to be complicated by characteristics of both magnetospheric and atmospheric obstacles.

Different types of "tails" form in the wakes of magnetospheric and atmospheric obstacles. The intrinsic field obstacle has a tail composed of stretched-out dipole field lines attached to the magnetic polar regions of the planet, while the atmospheric obstacle has a comet-like tail composed of interplanetary or solar-wind field lines which appear to have become hung up in the ionosphere as they slip around it. Moreover, the flowing solar wind has an associated electric field that removes the ionospheric ions produced in the upper atmosphere above the ionopause, creating both an upper boundary to the ionosphere and a wake of planetary ions. Intrinsic planetary fields often shield a planetary atmosphere against this type of solar-wind "scavenging" (although it can still occur if the magnetopause is low enough). Below, we will see how observations related to these and other features of the solar-wind interaction have been used to argue for and against appreciable Mars magnetism.

Our position to assess the situation at Mars has been improved considerably by the Pioneer Venus Orbiter. As a result of this long-lived mission with its low-altitude phase, we have an unprecedented picture of the atmospheric obstacle-solar wind interaction with which to compare our more inti-

mate knowledge of the terrestrial magnetic field obstacle-solar wind interaction. Analogies with Venus and Earth have formed the basis of many of the studies of the far more limited database for Mars. It will become clear that, at Mars, our understanding is, in the end, limited by our relatively inadequate *in situ* observations.

C. History of Measurements

Although there has recently been renewed activity in the space-based exploration of Mars with the launch of the two Phobos spacecraft (see the special Phobos issue of *Nature,* October, 1989), many earlier reviews of the results of Mars missions are still quite complete in terms of their scientific conclusions (see e.g., Vaisberg and Bogdanov 1974; Bogdanov and Vaisberg 1975; Russell 1979,1981; Intriligator and Smith 1979; Breus and Gringauz 1980; Slavin and Holzer 1982). Table I lists those missions during which *in situ* measurements of magnetic fields or other experiments with some direct relevance to the subjects of the magnetic field, ionosphere and solar-wind interaction have been carried out, including the latest Phobos 2 mission (Phobos 1 failed prior to arrival at Mars). Primarily because of radio-occultation experiments, which require minimal onboard experiment-specific instrumentation, this table constitutes a comprehensive list of almost all of the missions to Mars.

To get an idea of how thoroughly the space around Mars has been probed, it is useful to review the orbits of the spacecraft which made the *in situ* measurements. The spacecraft trajectory is typically displayed in a coordinate system where x is along the Mars-Sun direction and the orthogonal coordinate is the perpendicular distance of the spacecraft from that axis. Figure 3 contains a collection of such plots from various sources. From Fig. 3 and the periapsis altitudes in Table I, it is seen that, with rare exceptions, *in situ* data are not available from altitudes below ~800 km and from the wake region. The exceptions are the Viking mission Landers, which made direct ionospheric measurements during their entry although those measurements did not include the magnetic field, and Phobos 2, which was the first spacecraft to probe the central wake. Remote sensing measurements of the ionosphere by radio-occultation methods are possible whenever the line of sight between the spacecraft and the Earth intersects the ionosphere. However, this line-of-sight requirement does not permit coverage of the subsolar ionosphere (solar zenith angles ≤45°) or antisolar ionosphere because of the Mars-Earth-Sun geometry.

D. Organization of this Chapter

Central to the present chapter is the issue of the Martian intrinsic magnetic field. Although another chapter (chapter 5) deals with the details of the interior of Mars and its associated dynamo activity, a brief overview of the work that has been done on the subject, independent of solar-wind interaction

TABLE I
Summary of Mars Measurements Relevant to the Magnetic Field and Solar-Wind In

Spacecraft	Year of Encounter	Closest Approach	Relevant Instruments/ Experiments	Features Detected
Mariner 4 (USA)	1965	~13200 km (flyby)	magnetometer; energetic-particle detectors; radio-occulation experiment	bow shock; magnetosheath; ionosphere density profiles
Mariner 6, 7 (USA)	1970	flyby	radio-occulation experiment	ionosphere density profiles
Mars 2, 3 (USSR)	1971	~1100 km (orbiters)	magnetometer; ion/electron traps; plasma analyzer; radio-occultation experiment	bow shock; magnetosheath; planetary ion mantle; intrinsic field (?); ionosphere density profiles
Mariner 9 (USA)	1972	flyby	radio-occultation experiment	ionosphere density profiles
Mars 5 (USSR)	1974	~1800 km (orbiter)	magnetometer; ion/electron traps plasma analyzer; radio-occultation experiment	bow shock; magnetosheath; planetary ion wake; magnetotail (?); ionosphere density profiles
Viking 1, 2 (USA)	1976	Landers	retarding-potential analyzer; radio-occultation experiment	ionosphere density, temperature, composition profiles
Phobos 2 (USSR)	1989	~850 km (orbiter)	magnetometer; plasma composition analyzers; Langmuir probe; energetic particle detector; plasma wave detector	bow shock; magnetotail; planetary ion mantle and wake

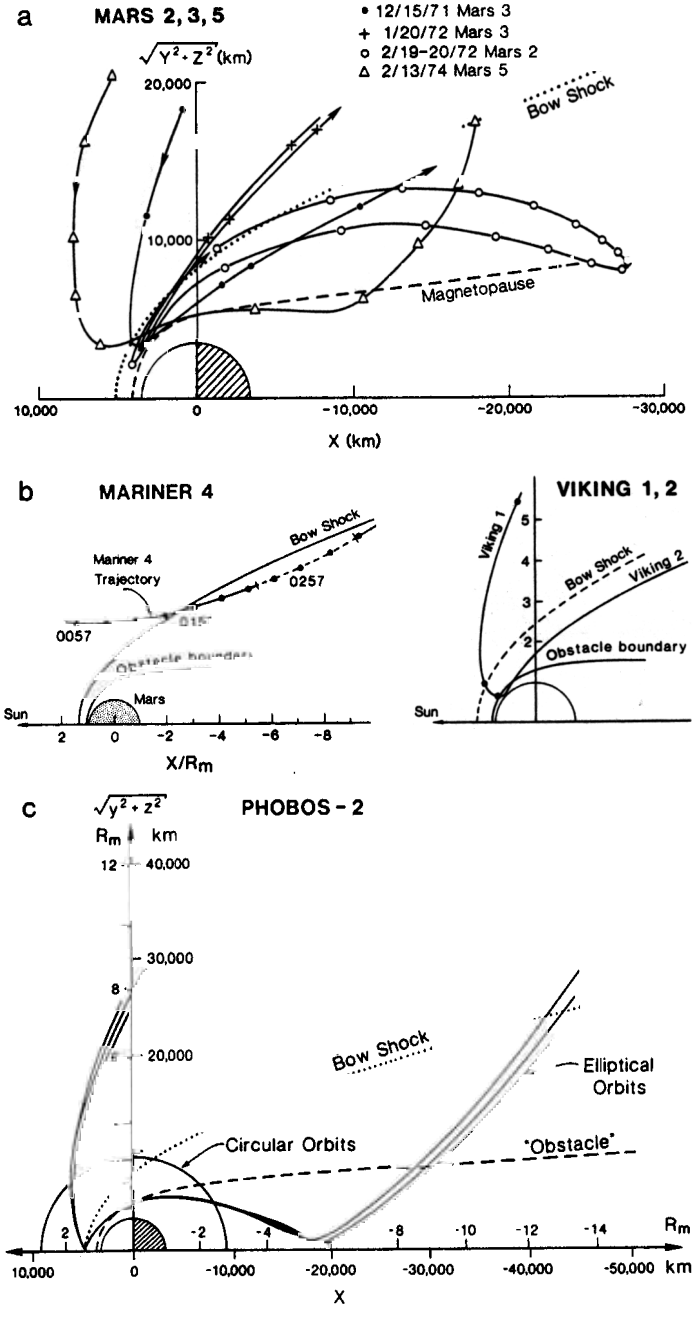

Fig. 3. (a) Examples of orbits of the Mars series of spacecraft in a cylindrical coordinate system where x points toward the Sun and $(y^2 + z^2)^{1/2}$ is the distance from the x axis. (b) Trajectories of the Mariner 4 flyby and Viking 1 and 2 Landers. (c) Trajectory of the Phobos 2 spacecraft during three of its elliptical orbits and in its circular orbit phase. Data from over 50 circular orbits were obtained.

observations and interpretations, is given here for the sake of perspective (Sec. II). This work deals principally with predictions based on dynamo theories of field generation in a rotating fluid sphere undergoing turbulent convection in its interior, and with theories concerning the properties of the cores of planets. A review of the inferences of Martian intrinsic magnetism from both *in situ* probes and meteorites follows.

The largest section of this chapter (Sec. III), like the largest proportion of published material, is devoted to the solar-wind interaction with Mars. The major features of the solar-wind interaction—the bow shock, magnetosheath, obstacle and tail, and their implications for the intrinsic magnetic field—are considered. Subsequent sections, which are devoted to the comparisons of Mars with Venus and Earth observations (Sec. III.G), emphasize the importance of comparative analyses in our ability to interpret what has been seen at Mars. Lastly, the related issues of the solar-wind interaction with the Martian satellites Phobos and Deimos are discussed with an eye toward their possible perturbations of the Mars environment (Sec. IV).

The discussion is selective in coverage as the aim of this chapter is to provide an overview of the current state of understanding of the subject and the basis for that understanding, rather than to provide an annotated bibliography. However, an effort has been made in the citations to maintain an accurate historical perspective.

II. MAGNETIC FIELD OF MARS

A. Dynamo Theory

For many years, in the absence of an adequate theory of planetary dynamos, it was conjectured that there was a "magnetic Bode's law," also called the Shuster or the Blackett hypothesis, which established that the magnetic moments of the planets (and stars) were proportional to their angular momenta (see Russell 1987). As shown in Fig. 4a, the magnetic moments of Jupiter and the Earth both fall on a line of proportionality on a plot of magnetic moment vs angular momentum if the angular momentum of the Earth-Moon system is used for the Earth. The fact that it is not obvious whether to use the angular momentum of the Earth or the Earth-Moon system is a clue to the lack of a physical basis for this hypothesis. The other planets with intrinsic fields lie significantly below (Saturn and Uranus) or significantly above (Mercury) the line. The two weakly magnetized planets (Mars and Venus) lie far below the line.

The concept of the dynamo generation of magnetic fields was first developed for the Earth (see review by Gubbins 1974). While no completely satisfactory dynamo theory currently exists, our present understanding suggests that the existence of a dynamo-generated planetary field requires rotation, an electrically conducting fluid core, and a significant source of energy in that core. It is thought that turbulent or nonaxisymmetric convection in the

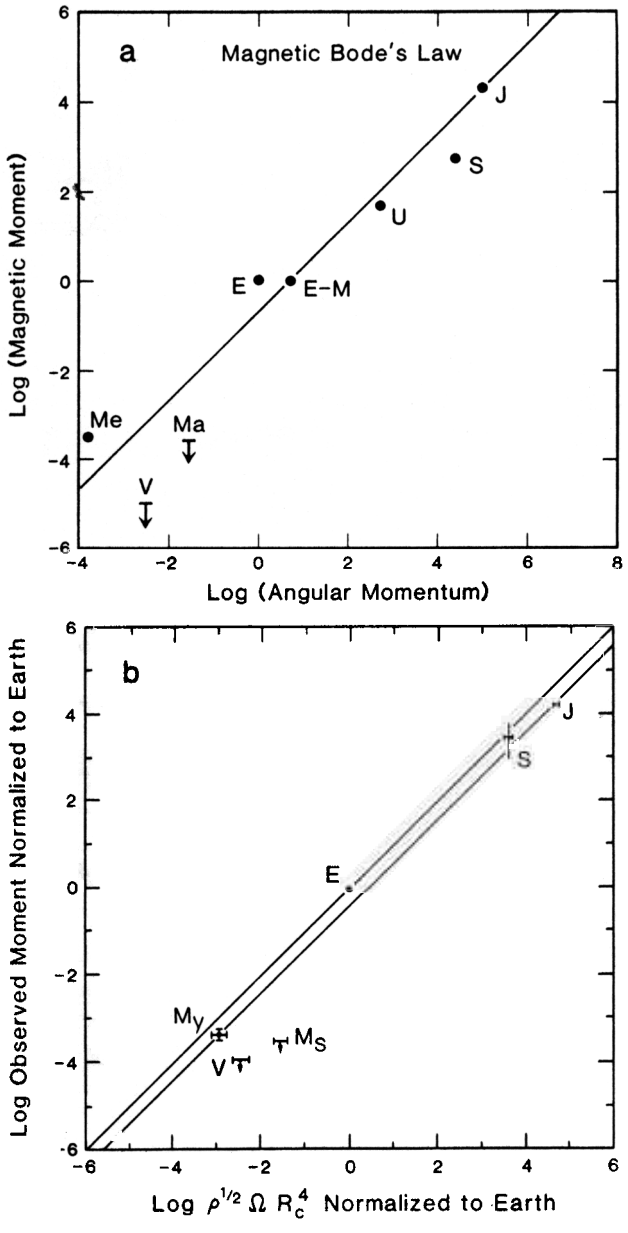

Fig. 4. (a) Original magnetic Bodes law relationship between planetary magnetic moment and angular momentum. (b) Dynamo theory-based modification derived by Busse (1976).

conducting core in the presence of rotation is essential to maintain the dynamo process. Busse (1976) applied one model of the dynamo process to create the physically based scaling law shown in Fig. 4b. This scaling law predicts that the planetary magnetic moment will be proportional to the rotation rate times the fourth power of the core radius. It is somewhat better at predicting magnetic moments than the original magnetic Bode's law. However, as before, Venus and Mars have magnetic moments far less than would be expected for active dynamos.

Planetary cores are quite inaccessible to empirical investigation by means other than modeling based on magnetic, seismic and gravitational measurements. Magnetic probing involves either theoretical interpretation of the measured intrinsic field in terms of dynamo models or electromagnetic "sounding" wherein the response of the near-planet field to interplanetary magnetic-field variability is measured (see Russell 1987). Seismic probing involves the inversion of seismographic data from instruments distributed on the planet's surface. As neither of these data sets are available for Mars, the properties of its core are estimated from other information. For example, the mean density of Mars, obtained from its radius and gravitational field, is only 3.9 g cm^{-3}, compared to 5.5 g cm^{-3} for Earth and 4.9 g cm^{-3} for Venus. If one presumes a mantle similar to that of the Earth, this implies a core radius of 1500 to 2000 km (Johnston and Toksoz 1977). Suggestions regarding the phase state and dynamical properties of the core range from a frozen core (Young and Schubert 1974) to a liquid core with minimal turbulent convection (Toksoz and Hsui 1978); however, these conclusions rely on the knowledge that the magnetic field is weak rather than on independent information about the core.

Because so little is known about the core of Mars, one is free to adjust its assumed properties constrained only by the size, mass, rotation rate and moment of inertia. Given these quantities, and the above core size estimate, the magnetic scaling law tells us that Mars should have a magnetic dipole moment of $\sim 10^{-2}$ times that of Earth if it behaves in a manner consistent with many of the other planets of the solar system. If Mars does not follow the trend of the other planets, it must have some distinctive internal properties that preclude the normal planetary dynamo action. As noted earlier, successful planetary dynamo operation requires an appropriately vigorous convection in the core and a long-lived internal energy or heat source to sustain that convection. In planets like the Earth, the most efficient source of energy for convective motion in the core is the release of gravitational and chemical energy during the course of formation of a solid inner core (Stevenson 1974; Stevenson et al. 1983). The conclusion is that Mars, which as we shall see has a "deficient" magnetic moment of $<10^{-4}$ that of Earth, is a planet with an entirely fluid or a completely solid core, or whose core solidification has ceased. Of course, it is possible that Mars had an active dynamo long ago, and if so, at least parts of the surface of Mars should possess remanent mag-

netization. However, it will be shown that remanent magnetization seems insufficient to play a major role in the solar-wind interaction with Mars.

B. Spacecraft Observations: Direct Observations

The first reports of the possible direct detection of a Martian magnetic field by a spacecraft experiment came from investigators analyzing data from the Soviet Mars spacecraft (see chapter 3). Dolginov and co-workers concluded that they observed the intrinsic field of Mars near the point of closest approach of the Mars 3 spacecraft (Dolginov 1976) and near the wake of the planet on the Mars 5 spacecraft (Dolginov 1978*a*). However, while supporting a detection of field lines directly connected to the planet, subsequent investigations made drastically different inferences as to the orientation and magnitude of the intrinsic field of Mars. For example, one analysis concluded that there was a feature similar to the Earth's magnetospheric cusp in the Mars 3 data, which implies a near-equatorial magnetic pole (Smirnov et al. 1978), while others resulted in the conclusion that the magnetic axis was nearly coincident with the rotation axis (see, e.g., Dolginov 1976). Meanwhile, the basic matter of the identification of the measured fields as planetary in origin was called into question by Wallis (1975) and Russell (1978*a,b*). The interpretations of these early observations continue to be controversial.

In particular, we know that no matter what the nature of the Mars obstacle to the solar wind is, it must have a magnetosheath as depicted in Fig. 1. As Wallis (1975) and Russell (1978*a,b*) have emphasized, allowance for the existence of this magnetosheath must be made in any accurate interpretation of the observed magnetic field. The magnetosheath field can also exhibit considerable structure and boundary-like features because the interplanetary magnetic-field orientation and strength are often variable, so particular care must be taken in determining the location of its inner boundary. One must accurately model the pile up of interplanetary magnetic field that occurs in a planetary magnetosheath to determine which features of the magnetic field observed at Mars *cannot* be explained by the solar-wind interaction. With one exception (see Russell et al. 1984), this was not done with the Mars spacecraft data. The latest Phobos 2 spacecraft magnetic observations, which provided unambiguous magnetotail data, indicate that at least above $\sim 2.7\ R_M$ the structure consists primarily of draped interplanetary fields as in the "induced" magnetotail of Venus (Riedler et al. 1989*a;* Yeroshenko et al. 1990). Thus, direct observations of a planetary field remain elusive.

C. Meteoritic Evidence

Three families of meteorites appear to have originated in the Martian crust. These are the Shergottites, Nakhlites and Chassigny, the so-called SNC meteorites. The evidence for their Martian origin has been reviewed by McSween (1985; see also chapter 4). The SNC meteorites are similar in mineralogy and chemistry to terrestrial rocks but have distinctive chemical and isotopic compositions. Trapped gases in Shergottite shock melts have compositions similar to those measured by the Viking spacecraft on Mars (Bogard and Johnson 1983) These meteorites were all ejected from their parent body relatively recently. They appear to have crystallized at shallow levels in the crust of their parent body ~1.3 Gyr ago or less from magmas produced by partial melting of previously fractionated source regions. All Shergottites appear to have experienced a shock ~180 Myr ago, which may be the time they were ejected into space following the impact of a large projectile. However, cosmic-ray exposure ages are significantly less than this, ranging from 0.5 to 2.4 Myr (Bogard et al. 1984). Since calculations indicate that 2/3 of the material reaching the Earth from a Martian ejection takes longer than 10 Myr to arrive (Wetherill 1984), these ages suggest that the meteorites spent much of their time in space as part of larger objects, perhaps >6 m in diameter.

Iron-bearing rocks like these meteorites acquire a natural thermal remanent magnetization when they cool through their blocking temperature in a magnetic field. They also can be magnetized when shocked or when sitting for long periods in a strong magnetic field such as that of the Earth. The latter magnetization should be "soft" and easily removed. Cooling in a background magnetic field should give a very "hard" remanent magnetization. A hard component of magnetization is found in some of the Shergottites. For the Shergottite EETA 79001, Collinson (1986) estimates the magnetizing paleofield intensity to be from 10^3 to 10^4 nT. For the Shergotty meteorite (the first Shergottite identified) itself, Cisowski (1986) estimates a paleofield strength of 250 to 1000 nT. While conceivably this hard remanence could have been imposed at the time of the shock event that liberated the meteorite from Mars, it seems more likely that the remanence was acquired at the time of crystallization 1.3 Gyr ago. Shock magnetization would require a significant magnetizing field much greater than the present-day limits on the global Martian magnetic field to be present only 180 Myr ago.

Of the estimates of paleointensity, the most certain appears to be that of Cisowski (1986), who used a modification of a particularly reliable method called the Thellier-Thellier technique. Even this technique does not prove that Mars had an active dynamo when the Shergotty meteorite crystallized, because a field as high as 250 nT could conceivably be provided by remanent magnetic fields acquired by the surrounding crust billions of years earlier. However, the most plausible, albeit by no means proven, explanation for the Shergotty paleointensity is the presence of an active dynamo 1.3 Gyr ago, when Mars was more geologically active, which generated a magnetic moment greater than 10^{13} T-m^3 (Earth has a moment of 8×10^{15} T-m^3). We note that the implied surface field strength of 250 to 1000 nT is more similar to that of Mercury than present-day surface fields of the Earth, Jupiter, Saturn or Uranus.

III. SOLAR-WIND INTERACTION

A. Solar Wind at the Orbit of Mars

The properties of the solar-wind plasma at the orbit of Mars at 1.5 AU heliocentric distance can be obtained by extrapolation of its well-determined parameters at 1 AU. The average radial velocity of ~400 km s^{-1} is expected to remain constant with radius. The density, which follows a $1/r^2$ law for the assumed spherical expansion, should be reduced to 1–2 ions cm^{-3} at Mars, while the proton temperature cools to $\sim 4 \times 10^4$ K. According to the Archimedean Spiral model of the interplanetary field, the magnetic field of ~1 to 5 nT should lie at an angle of ~ 56° from the Mars-Sun line, approximately in the ecliptic plane. These extrapolations have been more or less confirmed by plasma instruments on the Mars spacecraft (Gringauz et al. 1974,1976). If Mars was unprotected from the solar-wind, its cross section to the flow would intercept $\sim 5 \times 10^{25}$ solar-wind protons (of energies ~ keV) per second. As noted earlier, a critical quantity in defining the planetary obstacle is the solar-wind pressure. The incident momentum flux or dynamic pressure at Mars is nominally $\sim 9 \times 10^{-9}$ dyne cm^{-2} at the subsolar point, but this, like the other quantities, has a range of variability as suggested by Fig. 5, which was derived from measurements at Venus (Phillips et al. 1984) and scaled for Mars. The peak thermal pressure of the Martian ionosphere from the Viking Lander observations of Hanson and Mantas (1988) is shown on this figure for comparison. The solar-wind pressure usually exceeds the ionospheric thermal pressure at Mars, at least for the solar activity minimum conditions that the Viking Lander observations represented.

Of course, as at the Earth, the solar wind at Mars will be sporadically perturbed by the passage of interplanetary shock waves and other solar-wind disturbances. Mars will also be occasionally subjected to an influx of energetic (~10 keV to 10 MeV) ions and electrons associated with these shock waves or with flares on the Sun. These events are noteworthy because the weak Martian magnetic field cannot deflect the high-energy particles away from the planet as does the field at Earth; some will penetrate the thin Martian atmosphere and deposit the bulk of their energy in the planet's surface. The absorption of energetic particles was observed on Phobos 2 as a "shadow" or disappearance in their flux in the hemisphere opposite that where the unperturbed upstream interplanetary field would intersect the planet (Afonin et al. 1989).

B. Bow Shock

1. Observations. Probably the best-observed feature of the Mars-solar wind interaction, and the most-used intrinsic field strength diagnostic, is the bow shock: a standing magnetosonic wave in the solar-wind plasma that forms to force the solar wind to be slowed and diverted around an obstacle to its flow. The bow shock was easily observed in the solar-wind plasma upstream of the planet by both particle and field experiments on the various spacecraft visiting Mars; see, e.g., the reviews by Slavin and Holzer (1982) and Russell (1985). In fact, the bow-shock crossings observed in the data from the magnetic-field experiment on Mariner 4 (Smith et al. 1965), reproduced here in Fig. 6, were the first unambiguous indication of the small size of the Mars obstacle to the solar wind and hence the weakness of the Martian intrinsic field. The magnetometers detected the bow shock as a distinctive jump (of up to a factor of ~4) in the magnetic-field magnitude (Smith et al. 1965; Dolginov 1976,1978*a*). Particle experiments capable of detecting plasma at solar-wind energies saw corresponding sudden increases in density and temperature, and decreases in flow velocity (Vaisberg 1976*a*,*b*; Gringauz 1976). Other plasma experiments not designed for detecting protons of solar-wind energy (~keV) detected shock crossings as changes in their backgrounds (see, e.g., Cragin et al. 1982), which are sensitive to the properties of the plasma surrounding the spacecraft.

The various bow-shock observations at Mars collectively provide an indication of the shape of its surface of revolution as shown in Fig. 7. A standard precedure in bow-shock studies is to fit the shock data with a conic section curve of elliptical form:

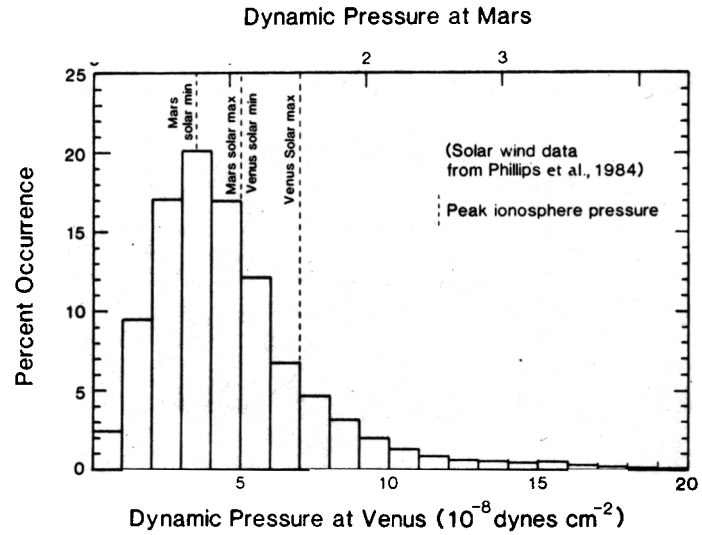

Fig. 5. Statistics of solar-wind dynamic pressure observed at Venus (bottom scale) and extrapolated to Mars (top scale). The dashed lines indicate how often the solar-wind pressure exceeds the peak ionospheric (thermal) pressure at both planets. The "Mars solar min(imum)" value was obtained from the Viking Lander measurements (Hanson and Mantas 1988). The peak thermal pressure at Venus at solar minimum should be comparable to that of Mars at solar maximum.

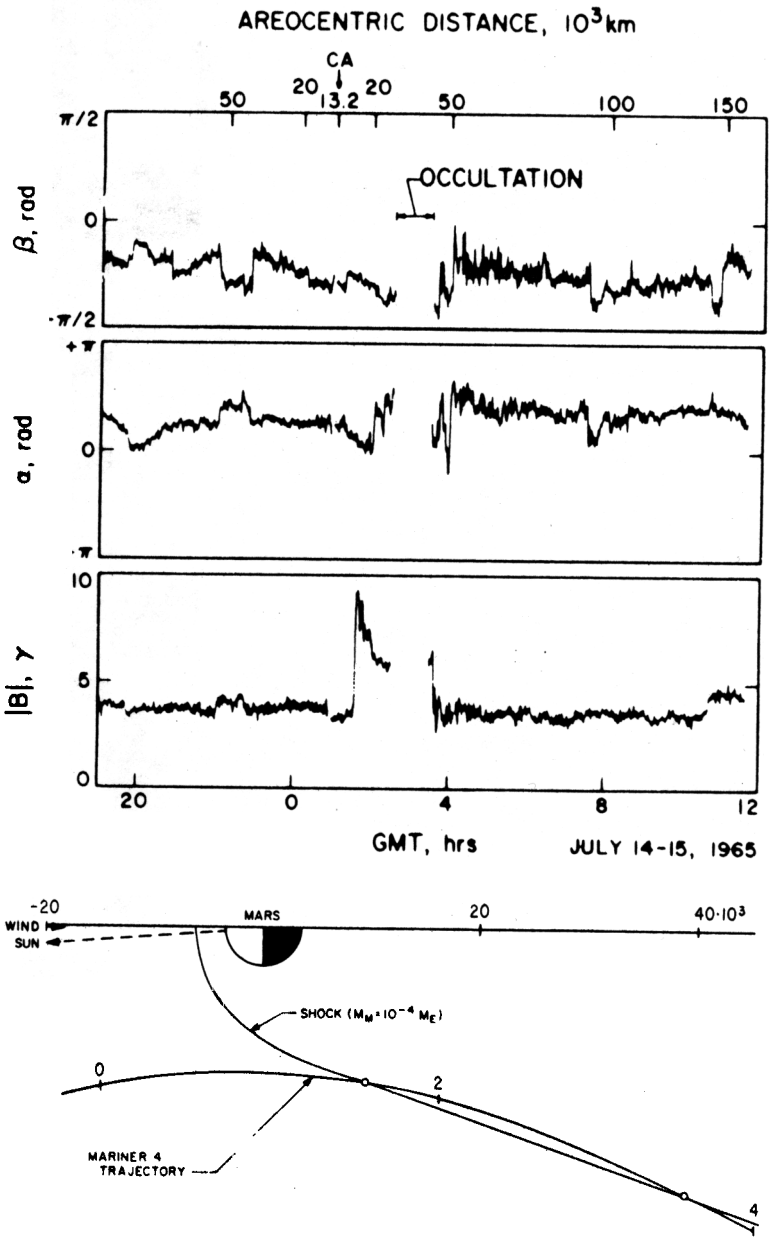

Fig. 6. First spacecraft observation of the perturbation of the solar wind by Mars. These magnetometer data from Smith et al. (1965) showed that the Martian obstacle to the solar wind must be on the order of the planet size. The panels show the polar and azimuthal angles of the field direction and the field magnitude. The spacecraft trajectory is labeled with GMT hr.

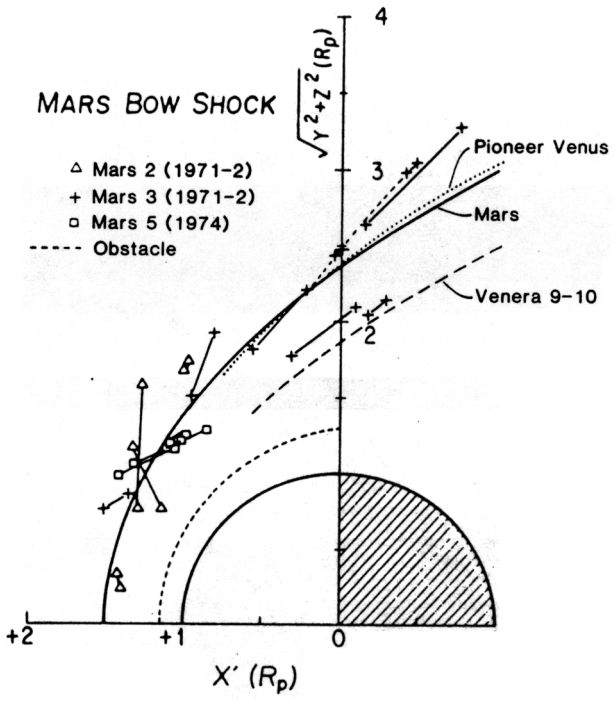

Fig. 7. Compilation of observed Martian bow-shock crossings adapted from Slavin and Holzer (1982) showing the best-fit conic section, the obstacle shape inferred from gas-dynamic models, and the relative positions of the Venus bow shock observed at solar maximum (from Pioneer Venus Orbiter) and minimum (from Venera).

$$R = \frac{K}{1 + \varepsilon \cos\theta} \tag{1}$$

where R is the radial distance from the center of Mars, K is the semi-latus rectum or radius of the shock at the terminator (day-night boundary) plane, ε is the eccentricity, and θ is the solar zenith angle (the angle between the Mars-Sun line and the radius vector to the point of interest). Many investigations have used curves of this form to fit the bow-shock data (see, e.g., Slavin and Holzer 1981,1982; Slavin et al. 1983; Russell 1985); however, as the authors of these studies noted, the inferred shape is subject to orbital sampling bias. In the most recent study by Slavin and Holzer (1982), care was taken to eliminate those shock crossings farthest from the Sun, which the investigators felt were the most strongly biased. Their best-fit curve, shown superposed on the data in Fig. 7, has an eccentricity of 0.94 and a semi-latus rectum of 1.94 planetary radii. These values were derived with the additional assumption that the origin could be moved from the center of Mars. Thus, they refer to a

coordinate system with its origin 0.5 planetary radii in front of the center of Mars so that $K = 1.94\ R_M$ is the distance from the x axis at $x = 0.5\ R_M$ (instead of the terminator plane $x = 0$). As seen in Fig. 7, their subsolar shock position is at $\sim x = 1.5\ R_M$ and the terminator shock is at $\sim 2.4\ R_M$. Using essentially the same data, Vaisberg et al. (1976) derived a shock that was closer to the subsolar point by $\sim 0.1\ R_M$. The most recent observations from Phobos 2 show that at encounter the subsolar distance of the bow shock from the center of Mars was also $\sim 1.5\ R_M$, but the terminator distance was $\sim 2.7\ R_M$ (Schwingenschuh et al. 1990). The terminator-radius difference could be related to the effect of the level of solar activity (which we discuss below).

2. Gas-Dynamic Models. Another standard procedure in studies of the bow-shock shape is to compare the empirically determined shape with models of shocks formed by hypersonic hydrodynamic or gas-dynamic flow around cylindrically symmetric obstacles. The pioneers in this area were Spreiter and his co-workers, who first used the hypersonic-flow analogy for the bow shock of the Earth; later it was applied to the Mariner 4 observations (Spreiter and Rizzi 1972; also see Dryer and Heckman 1967) for the purpose of deducing the obstacle size at Mars and hence inferring its intrinsic field strength.

The reason why the gas-dynamic flow analogy is applicable to magnetosonic bow shocks is that the effect of the magnetic field on the shock (which is what distinguishes it from a gas-dynamic shock) is negligible when the upstream Alfvén Mach number (the square root of the ratio of plasma kinetic-energy density to the magnetic-energy density) is ≥ 8. Under these circumstances, one can simply assume that the magnetic field is convected and compressed with the flow. At Mars, the magnetosonic Mach number (the square root of the ratio of plasma kinetic-energy density to the thermal plus magnetic-energy density) of ~ 7 justifies the use of this approximation and hence the use of the gas-dynamic model to infer the obstacle size and shape.

From their early analyses of the Mariner 4 shock observations, Spreiter and Rizzi concluded that the size of the Mars obstacle to the solar wind was consistent with what would be expected if the planetary ionosphere alone deflected the flow (also see Spreiter et al. 1970). As mentioned in the introduction, the key to determining the obstacle is the consideration of pressure balance of the solar-wind pressure by either magnetic pressure ($B^2/8\pi$, where B is the field in nT and the pressure is in dyne cm^{-2}), plasma thermal pressure (nkT, where n is density, k is Boltzmann's constant and T is the sum of the ion and electron temperatures, all in cgs units), or a combination of both. The solar-wind pressure can be evaluated in the upstream region where it is practically all dynamic pressure (ρV^2 where ρ is mass density and V is the flow speed) with a correction for the angle of incidence (as only the pressure normal to the boundary surface matters in the obstacle determination). The authors calculated an obstacle shape for an ionosphere with a constant scale

height (e.g., with a pressure profile that decreases exponentially with altitude) and then calculated the shock shape that it would produce. Thus, in order to conclude that the observed shock was consistent with an ionospheric obstacle, they had to make some assumptions about the ionosphere. Guidance was provided by the radio-occultation experiment on Mariner 4, which gave information about the ionospheric electron densities and plasma temperatures (from the scale height).

In the same way, more definitive assessments of the obstacle shape were made later, as the statistics from other spacecraft measurements better defined the shock shape. In the most recent study by Slavin and Holzer (1982), mentioned above, gas-dynamic models from a library of calculations carried out by Spreiter and Stahara (1980) were compared to the collected shock data. Their best fit, for a Mach number 7.2 and normalized scale-height obstacle shape factor H/r_o of 0.03, is shown in Fig. 7. As the authors noted, the obstacle for this case, also shown in Fig. 7, has a subsolar altitude of ~ 400 km. At the time that this result was obtained, the Viking Landers had measured the ionospheric electron density and ion temperature along two trajectories through the dayside ionosphere. In addition to the observation that a negligible ionospheric plasma density remained at 400 km, the measured ion temperature and an inferred electron temperature of twice that value gave a pressure at that altitude of $<50\%$ of the estimated incident solar-wind pressure. Thus, in contrast to the earlier analysis by Spreiter and Rizzi, this latest study concluded that the obstacle size inferred from the observed bow-shock shape and gas-dynamic models could *not* be produced by the ionosphere alone. Slavin and Holzer further deduced that the magnetic dipole moment that would produce a field sufficient to balance the average solar-wind dynamic pressure at Mars at 400 km subsolar altitude was 1.4×10^{22} G cm^{-3} or 1.4×10^{12} T-m^{-3}. This conclusion was roughly consistent with the results derived in the host of intervening studies based on similar arguments, the history of which is illustrated in Fig. 8. (The three high values at the outset were deduced from the observed absence of trapped energetic particles on Mariner 4 instead of from the shock position.) Similar results obtained from fitting the Phobos 2 bow shock have now further corroborated these earlier estimates of the subsolar obstacle altitude and inferred intrinsic field strength (Riedler et al. 1989*a*; Schwingenschuh et al. 1990).

C. Magnetosheath: Observations and Gas-Dynamic Models

In the previous discussion of the interpretation of the Mars spacecraft magnetic-field data in terms of an intrinsic field, we emphasized the importance of accurately modeling the draped magnetosheath magnetic field. The same gas dynamic model used in studies of the bow shock data is appropriate for this purpose, but only one investigation (Russell et al. 1984) applied the model accordingly. The result of that effort is illustrated in Fig. 9, which shows the authors' favorable comparison between the model and the Mars 5

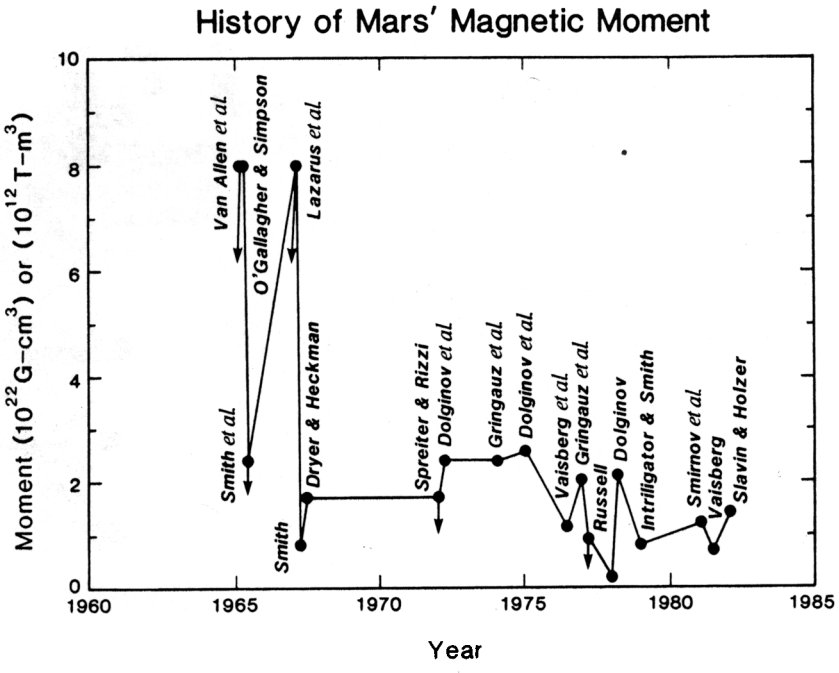

Fig. 8. Time history of the dipole magnetic moment of Mars inferred from spacecraft data

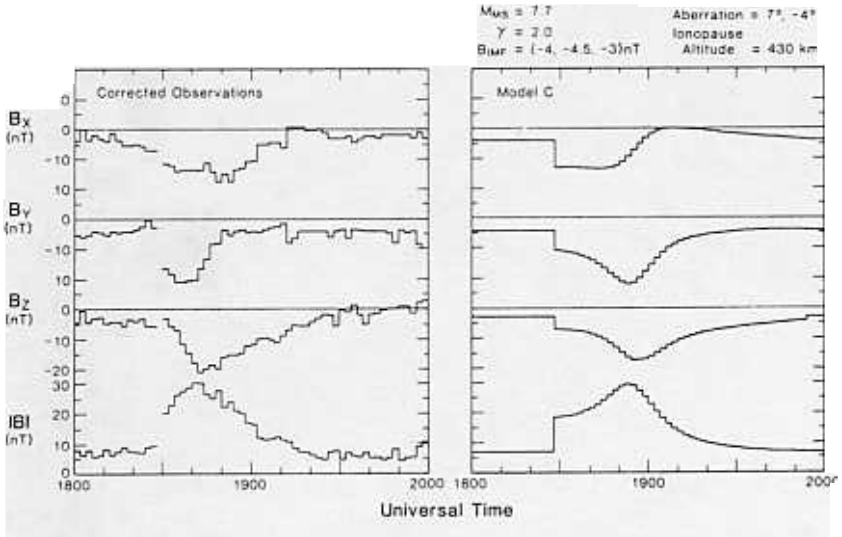

Fig. 9. Comparison of the magnetic-field vectors measured during a passage of the Mars 5 spacecraft through the Mars magnetosheath with a simulation of the interval using a gas-dynamic model (figure from Russell et al. 1984).

data. However, this comparison has been criticized by the Mars 5 principal investigator because it involved a rotation of the coordinate system of the magnetic field observations inconsistent with his own assessment (Dolginov 1986; see also Russell 1986). Nevertheless, we know both from observations outside the magnetospheric obstacle of Earth (Crooker et al. 1985), and from observations above the ionospheric obstacle of Venus (Luhmann et al. 1986*a*) that the gas-dynamic model should provide a good description of the magnetic field draping around Mars under steady solar-wind and interplanetary-field conditions regardless of the nature of the obstacle. Practically the only exception, besides that of disturbed interplanetary conditions, should be when the interplanetary field is aligned with the solar-wind velocity. Under such circumstances, the magnetosheath magnetic field will appear turbulent because of the turbulent nature of the subsolar bow shock when the upstream field is normal to its surface (a characteristic of this type of shock which is referred to as a "quasiparallel" shock) (see Luhmann et al. 1983). However, this condition is likely to be rarer at Mars than at Venus or Earth, because the oblique angle of the magnetic field increases with distance from the Sun.

An analogous comparison of the plasma data from Mars-5 with a gas-dynamic model is shown in Fig. 10. Although this is the only example available where such a comparison with plasma data was made, it illustrates the extent to which the magnetosheath-model variations in velocity and temper-

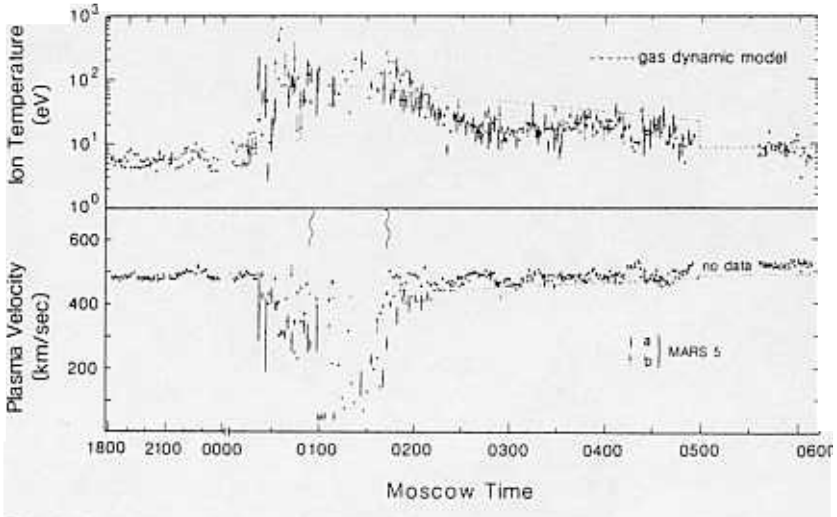

Fig. 10. Comparison of an interval of Mars 5 plasma data with a gas-dynamic model. The wavy lines mark the interval of disagreement that is considered evidence of entry into the Martian "magnetosphere." The closed symbols (a) are from the sensor that detected both light and heavy ions, while the open symbols (b) are from the sensor that detected light ions only. (The data are from Vaisberg et al. 1976*a*.)

ature along the spacecraft trajectory agree with the observations. As in the case of the magnetic field, such comparisons are particularly valuable for evaluating those plasma measurements that reportedly show evidence of passage into the obstacle. For example, the interval of disagreement in Fig. 10 marked by the wavy lines was considered evidence of entry into the Martian "magnetosphere" (Vaisberg et al. 1976*a*).

In spite of their success, gas-dynamic models of planetary magnetosheaths are expected ultimately to fail to describe the observations on several scores. One problem area is in the innermost layer of the magnetosheath where the convected, draped interplanetary magnetic field piles up to an extent that the field strength exerts control over the flow of the compressed solar-wind plasma. In this magnetic "barrier" or magnetic "cushion" region, one expects to find a depleted plasma density which is not predicted by the gas-dynamic frozen-field model (Zwan and Wolf 1976). Furthermore, in both the barrier and in an extended region of the magnetosheath, heavy planetary ions like O^+ will be produced by photoionization of that part of the neutral exosphere that extends above the obstacle boundary (Nagy and Cravens 1988). Impact ionization of these particles by solar-wind particles and charge exchange between solar-wind protons and the neutral atoms also add to the ion population (Russell et al. 1983). These processes constitute a source of mass in the magnetosheath plasma flow. The effects of mass loading on the shape of the bow shock have been shown to be significant at Venus (Alexander and Russell 1985), where the shock is found to be at larger distances from the planet than expected for an obstacle in the shape of Venus' ionopause, and its position depends on the ionizing solar EUV flux. Gas-dynamic models which include a source of mass have been developed (cf. Breus 1986; Berlotserkovskii et al. 1987), but these do not take into account some important physical details such as the manner in which the heavy ions are incorporated into the flow. A possible conceptual explanation of the solar-cycle effect could be that the barrier region, not the ionopause, forms the effective obstacle, and that the barrier size depends on the amount of mass addition. Thus it is notable that observations at Mars with the plasma analyzers on both the Mars 2 and Mars 3 spacecraft indicated the presence of a region of slowly moving plasma and increased magnetic field strength at approximately the location of the obstacle that would produce the observed bow-shock shape (Vaisberg 1976; Vaisberg et al. 1990). The existence of this barrier region provides an explanation for the interval of disagreement with the gas-dynamic model identified in Fig. 10. The detection of an inner boundary of the solar plasma at ~2000 km altitude near the terminator (Vaisberg and Smirnov 1986), and of heavy ions (possibly O^+) in a tail boundary layer illustrated in Fig. 11 by detectors on Mars 5 (Vaisberg et al. 1976*a*,*b*) was also reported. Although the heavy-ion interpretation of the early plasma data was contested (Bezrukikh et al. 1978), these observations taken together with the dayside observations are consistent with the idea that a planetary ion-laden mantle,

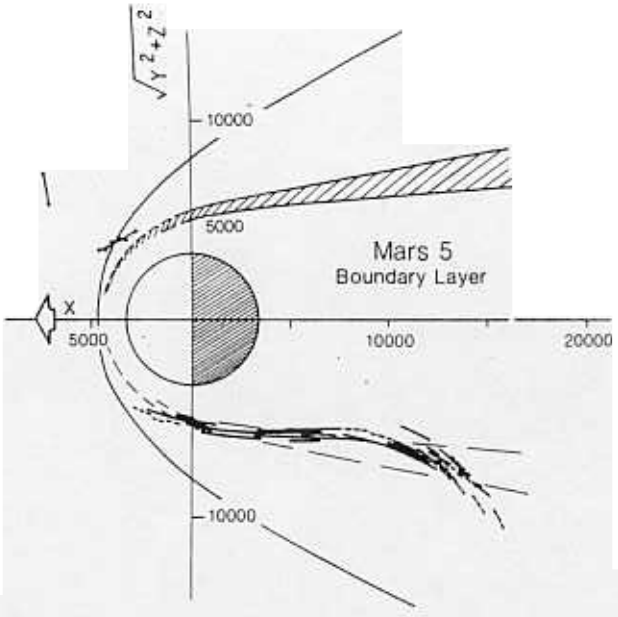

Fig. 11. Sketch of the location of the magnetosheath/magnetotail boundary layer suggested by plasma measurements on Mars 5 (figure from Vaisberg et al. 1976*a*,*b*).

threaded by stagnating piled up interplanetary field, determines the obstacle shape at Mars. Moreover, this picture is now reinforced by Phobos 2 results, which unambiguously show a heavy O^+ ion layer in the inner magnetosheath around which the solar-wind plasma appears to be deflected (Lundin et al. 1989; Rosenbauer et al. 1989; Riedler et al. 1989*a*). The outer boundary of this layer has been called the planetopause.

One aspect of mass loading that the modified gas-dynamic models do not include is related to the details of how at least some of the planetary ions are "picked up" by the solar wind. A convection electric field is associated with the moving magnetized solar-wind plasma. This field is distorted but persists in the magnetosheath where the solar-wind flow is diverted around the obstacle. If there is no turbulence in the magnetosheath to scatter the ions, they are smoothly accelerated by the electric field to energies that oscillate between zero and the kinetic energy associated with up to twice the velocity of the background flow. The important consideration here is the cycloidal geometry of their trajectories as they are accelerated. Planetary ions like O^+ are so heavy that their gyroradii can be comparable to or larger than the diameter of Mars. Thus, their trajectories can take them either into the lower atmosphere where they are absorbed or outward and tailward where they escape from the planet (Cloutier et al. 1974; Wallis 1982). The approximate appearance of the resulting "pickup ion exosphere" and associated "ion tail"

can be examined by calculating the motions of test particles in the gas-dynamic magnetosheath magnetic field and convection electric field model. Figure 12 illustrates the behavior of exospheric O^+ ions near Mars that are expected to form an asymmetrical ion tail as a result of this finite gyroradius effect. Luhmann and Schwingenschuh (1990) and Luhmann (1990) discuss the energy distributions of these ions, some of which are accelerated almost as if they were in the unperturbed solar wind (with a nominal maximum energy of ~60 keV for an interplanetary field perpendicular to the velocity), while others which are diverted into the wake attain much lower energies. The Phobos 2 observations show that there are copious fluxes of planetary ions in the magnetosheath and wake of Mars (Lundin et al. 1990*a*,*b*; Rosenbauer et al. 1990), although it is not yet known whether their properties are consistent with the model in Fig. 12. In any case, the consequences of such a population on the flow and field may need to be considered when applying unperturbed gas-dynamic models to observations around Mars.

In a similar vein, kinetic treatments of at least the solar-wind protons may be necessary for studying the solar-wind interaction itself since the scale of the proton gyroradius can be comparable to the thickness of the subsolar Martian magnetosheath. In addition to a thick "foot" upstream of the subsolar shock (Moses et al. 1988), solar-proton absorption in the lower atmosphere analogous to the absorption of the pick-up ions can occur. The details of the effects of such finite proton gyroradius scaling on the bow shock and magnetosheath can be deduced only through the application of models such as global hybrid models of the solar-wind interaction which are currently under development (Brecht 1989). In the meantime, the favorable comparisons between the gross features of the gas-dynamic models and the observations mentioned above indicate that for many purposes, they can be used to describe the bulk plasma and field behavior around Mars.

D. Aeronomical Consequences of the Solar-Wind Interaction

This book includes a separate chapter on the aeronomy of Mars (chapter 30), but, as was the case for the planetary dynamo, it is appropriate to review here those aspects of Martian aeronomy that pertain to the intrinsic magnetic field and solar-wind interaction. The subjects of interest in the present context are the observed aeronomical properties of Mars, in particular of its ionosphere, that tell us about the local magnetic field, and the effects, both long-term and short-term, of the solar-wind interaction on the atmosphere.

1. Ionosphere Observations: Viking Landers. The only *in situ* measurements of the Martian ionosphere are from the retarding potential analyzers on the two Viking Landers (Hanson et al. 1977). These instruments provided altitude profiles of the electron and ion density, ion composition, ion and electron temperatures, and ion velocities at two dayside locations during conditions of low solar activity. The collected data on densities and tempera-

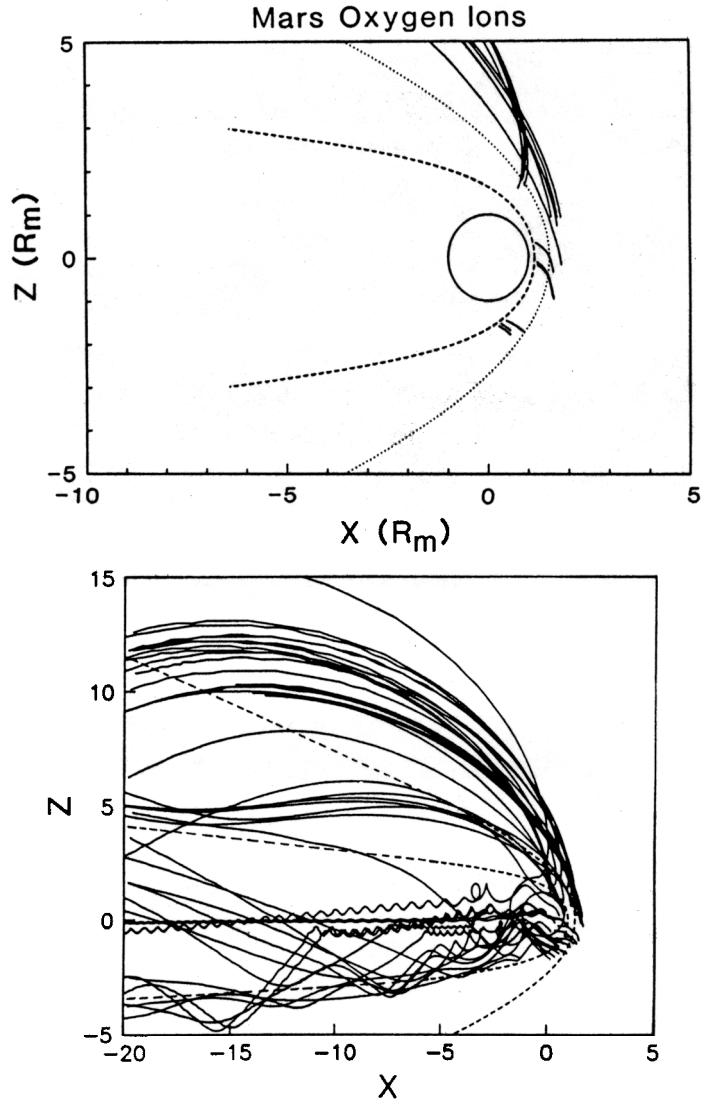

Fig. 12. Calculated trajectories (noon-midnight plane projections) of planetary O^+ ions picked up by the solar wind flowing past Mars. The upper frame shows representative trajectories outside of the obstacle surface, which either intersect the obstacle or reach large distances above the obstacle surface as the ion undergoes cycloidal motion. These were calculated using the magnetosheath-field model of Spreiter and Stahara (1980). The lower frame shows some trajectories from a model which includes a magnetic-field model for the wake inside of the obstacle (figure from Luhmann 1990).

tures are displayed in Figs. 9, 11 and 12 of chapter 30. As mentioned earlier in the discussion of the bow-shock shape, these data were used to compute the thermal-plasma pressure for comparison with the nominal solar wind pressure at Mars (Intriligator and Smith 1979; Slavin and Holzer 1982). The conclusion, reached even before the Viking investigators published their results on the electron temperatures (Hanson and Mantas 1988), was that during the Viking entry observations, the solar-wind pressure exceeded the thermal pressure of the Martian ionospheric plasma at the inferred obstacle altitude. The final thermal pressure profile deduced by Hanson and Mantas (1988) is shown in Fig. 13 where the average solar-wind pressure (see Fig. 5) is also noted. As the bow-shock studies indicated that the subsolar obstacle should be located near 400-km altitude, the weak ionosphere presented a problem that these early authors sought to solve by invoking the internal pressure of an intrinsic magnetic field of Mars. The absence of clear evidence of an ionopause in the Viking Lander density profiles strengthened their conviction that the ionosphere of Mars was magnetically protected from direct solar-wind influence. The ion velocity data were not conclusive because they showed a variability with altitude that was not consistent with any of the proposed models for magnetospheric or plasmaspheric convection (Bauer and Hartle 1973; Rassbach et al. 1974).

Several other analyses of the Viking Lander data yielded evidence for a magnetic field in the Martian ionosphere. Chen et al. (1978), Johnson (1978) and Rohrbach et al. (1979) used ionospheric models based on the Lander observations of the neutral atmosphere to argue that the ion temperatures

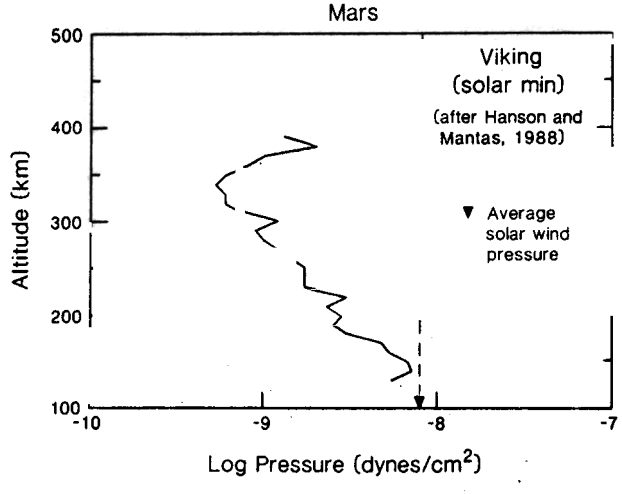

Fig. 13. Altitude profile of the thermal plasma pressure in the Martian dayside ionosphere as measured on the Viking Landers (figure adapted from Hanson and Mantas 1988). The dashed line denotes the typical solar-wind dynamic pressure at Mars. The Viking Landers arrived at Mars during a period of minimum solar activity.

measured on the probes were too large to be produced by solar radiation incident on a field-free atmosphere. By introducing near-horizontal fields of 10s of nT to inhibit vertical heat transport, they were able to approach more nearly the observed ion temperature gradients. Hanson and Mantas (1988), in their recent analysis of the electron temperature data, reached the same conclusion. However, all authors agreed that it is not possible to determine whether the required field was intrinsic or somehow induced by the solar-wind interaction. It is also not possible to rule out a contribution to the observed gradients by either local or topside heating of some kind (e.g., see Taylor et al. 1979).

The matter of induced ionospheric magnetic fields will come up again when we discuss the analogy with Venus (Sec. III.F). Models of induced magnetic fields in the ionospheres of the weakly magnetized planets, including Mars, had been formulated even before the Viking mission data were obtained (Cloutier and Daniell 1973). These fields were envisioned to be related to currents driven by solar-wind electric fields imposed across the ionosphere because the atmosphere absorbed a fraction of the incident solar wind (also see Cloutier and Daniell 1979). After the Pioneer Venus mission showed that induced fields, whatever their nature, were indeed present at Venus (Russell et al. 1979; Elphic et al. 1980), Slavin and Holzer (1982) "revisited" the inferred obstacle-size problem, asking the question of whether a Venus-like induced ionospheric field pressure could combine with the thermal pressure of the Martian ionosphere to produce the inferred obstacle at 400 km altitude. Their answer was negative, but, as we shall see later, that conclusion was premature based on later analyses of the Venus results (Luhmann et al. 1987). Thus the interpretation of the Viking measurements of the Martian ionosphere and their implications for an intrinsic magnetic field remain unresolved, largely because a magnetometer was not included on the Landers. Nevertheless, from the Landers we obtained two key pieces of information of interest to the present chapter. These concerned the magnitude of the ionospheric thermal pressure at Mars, and the inference of a large-inclination magnetic field of some 10s of nT in the ionosphere from the measurements of the plasma temperature gradients.

2. Ionosphere Observations: Radio Occultation Experiments. Radio-occultation techniques provide us with the most widespread coverage of the Martian ionosphere, spanning the solar zenith-angle range from ~42° to 138°. Virtually every mission to Mars (see Table I) has returned radio-occultation altitude profiles of electron density. This history allows us to examine such questions as the solar-cycle variability of the ionosphere; however, from the viewpoint of studying the solar-wind interaction, analyses of these data have been minimal. Because no ionopause-like boundary features were clearly distinguishable in the Mars radio-occultation profiles (Kliore et al. 1972; Lindal et al. 1979), efforts have generally concentrated instead on

the behavior of the electron density peak and the near-peak topside scale heights that tell us something about the neutral atmosphere (see, e.g., Fjeldbo and Eshleman 1968; Fjeldbo et al. 1970; Hogan et al. 1972; Kliore et al. 1972,1973; Lindal et al. 1979).

Except for an early attempt by Cloutier et al. (1969) to attribute the observed small topside ionosphere scale heights to solar-wind effects, which turned out to be unnecessary (see Hogan et al. 1972), Slavin and Holzer (1982) presented one of the first analyses of radio-occultation results aimed at addressing the solar-wind interaction problem. Using the electron density profiles available in the literature, they mapped the altitude of the "top" of the Martian ionosphere as a function of solar zenith angle (a study impossible with the available *in situ* data). Their result, reproduced here in Fig. 14, illustrated that the top of the ionosphere, so defined, was several 100s of km lower than the Mars obstacle altitude inferred from the observed bow-shock position and gas-dynamic models. These data were interpreted as further support for their intrinsic magnetic field argument. With such results by themselves, this conclusion was natural, but it must also be considered in light of the Venus observations, where neither the solar-minimum or solar-maximum shock position can be produced by an obstacle shaped like the ionopause. In any case, the archive of radio-occultation data may still contain some results of value for solar-wind interaction studies (e.g., see Zhang et al. 1990*a*,*b*).

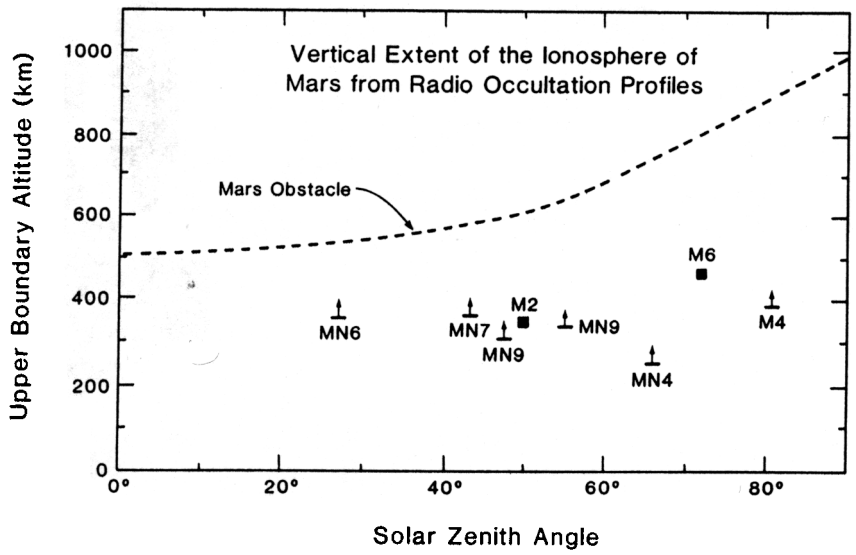

Fig. 14. Locations of the top of the Martian ionosphere from radio-occultation profiles compared to the obstacle height inferred from the bow-shock observations (figure from Slavin and Holzer 1982).

3. Implications for Neutral Atmosphere Evolution. Whether or not Mars has an intrinsic magnetic field of significance to the solar-wind interaction, Mars still presents little more than a planet-sized obstacle to the solar-wind flow as inferred from the observed bow-shock shape. Nagy and Cravens (1988) and Ip (1988) recently constructed models of the Martian neutral exospheres of oxygen and hydrogen that show these exospheres extend well above the 400-km inferred subsolar obstacle altitude. This means that, unlike the situation at Earth and like that at Venus, the particles in the upper neutral atmosphere at Mars can be ionized and "picked up" by the solar wind and magnetosheath convection electric field as described earlier. The picked-up ions illustrated in Fig. 12 constitute a source of mass for the solar wind, but a sink for the neutral atmosphere.

One can estimate the amount of solar-wind scavenging that occurs on time scales of the age of the solar system by integrating the total number of photoions produced per unit time from exospheric neutrals above the obstacle boundary and multiplying by 4.5 Gyr. Of course this presumes that all of the ions produced are indeed carried away from the planet (for a discussion of a possible limit see Michel [1971]), and that the exosphere, solar-ionizing radiation, and solar wind have been constant over this long time period. This loss mechanism applies to all constituents of the upper atmosphere, but the constituents of water are of special interest because the weakly magnetized planets seem to have a shortage of it. For a model exosphere of the type proposed by Nagy and Cravens (1988), a photoionization rate of 4×10^{-7} s^{-1}, and an obstacle located at ~400 km altitude over the dayside hemisphere, roughly 10^{23} oxygen ions s^{-1} and 10^{24} hydrogen ions s^{-1} are removed from Mars by the solar wind. Over 4.5 Gyr, the lost oxygen is enough to have contributed to under a meter of water over the planet's surface. The facts that other ionization mechanisms such as impact by solar-wind electrons and charge exchange between protons and neutrals are thought to increase the ion production rate by ~ a few times, and that the exosphere density is uncertain by at least a factor of ~5 (see Ip 1988), make this a conservative estimate. Moreover, if the exosphere was once hotter, and therefore more extensive, or if the ionizing solar photon flux was higher, these numbers could have once been considerably larger, making this mechanism much more significant in determining the present composition of the Martian atmosphere (e.g., see McElroy et al. 1977). On the other hand, a colder exosphere or lower ionizing solar-photon flux in the past, a historically weaker solar-wind dynamic pressure, or a substantial intrinsic magnetic field from some long-ago dynamo activity in the Martian core, would limit its effectiveness. There are also other solar wind scavenging mechanisms that one could propose (see, e.g., Brace et al. 1987; Perez-de-Tejada 1987), which may be necessary if the Mars/Phobos 2 spacecraft investigators' estimates of oxygen ion-loss rates of $\sim 10^{25}$ s^{-1} (Vaisberg 1976; Lundin et al. 1989; Rosenbauer et al. 1989) are accurate. With our lack of knowledge of the past Martian exosphere and intrinsic field,

and of the history of the solar wind, we are left to speculate as to whether the weakness of the magnetic field of Mars is intimately connected with the current state of its atmosphere (e.g., see McElroy et al. 1977; Cordell 1980). Nevertheless, the Phobos 2 observations tell us something about the present ion-scavenging loss rates.

Some alternative evaporative escape processes that remove *neutral* constituents of the exosphere have little to do with the solar wind (cf. McElroy 1972; Hunten and Donahue 1976; Wallis 1978), but Watson et al. (1980) proposed that sputtering of the atmosphere by solar-wind particles reaching the Martian exobase (at ~200 km) could also have provided a significant loss of atmospheric neutrals over time. These authors suggested that this mechanism might be particularly important for explaining some of the anomalous isotope and rare-gas abundances observed in spectroscopic studies of the Martian atmosphere. However, all of the aforementioned studies indicate that, at least at present, the bulk of the solar-wind plasma is effectively slowed and deflected around Mars. On the other hand, this does not rule out the possible importance of sputtering by the accelerated pick-up ions that impact the lower atmosphere (Luhmann and Kozyra 1991). Measurements at Mars pertaining to the loss of neutrals such as oxygen and its causes remain to be done.

E. Wake and Tail

1. Models. A number of models have been proposed for the origin and configuration of the Martian magnetotail. As none of these have been developed to the point where they are numerical or analytical, they are generally presented in the form of cartoons showing the source of the field lines that extend into the wake of the planet. Figure 15 displays three that have appeared in the literature. A schematic of Venus' "induced" magnetotail, which presents another alternative for Mars, is shown in the upper left for contrast. As one can see, virtually all of the models proposed for Mars in the past incorporated a planetary dipole field.

2. Observations. The orbit diagrams in Fig. 3 best communicate the marginal quality of the presently available observations of the Martian wake and tail prior to the Phobos 2 mission. Nevertheless, the Mars 5 spacecraft missions produced the result in Fig. 16, which is a map of a "tail boundary." The identification of this boundary is based on observations of a transition in plasma properties suggesting a passage from a hot, rapidly flowing magnetosheath plasma to a cooler, more slowly flowing medium (Vaisberg and Smirnov 1986). As mentioned earlier, a layer of heavy ions has also been reported in the vicinity. A similarly shaped boundary was identified by Dolginov et al. (1976) on the basis of magnetic measurements. While these observations may indeed be of the Mars tail boundary or of the innermost edge of the magnetosheath, it is quite likely that they suffered from an orbital bias

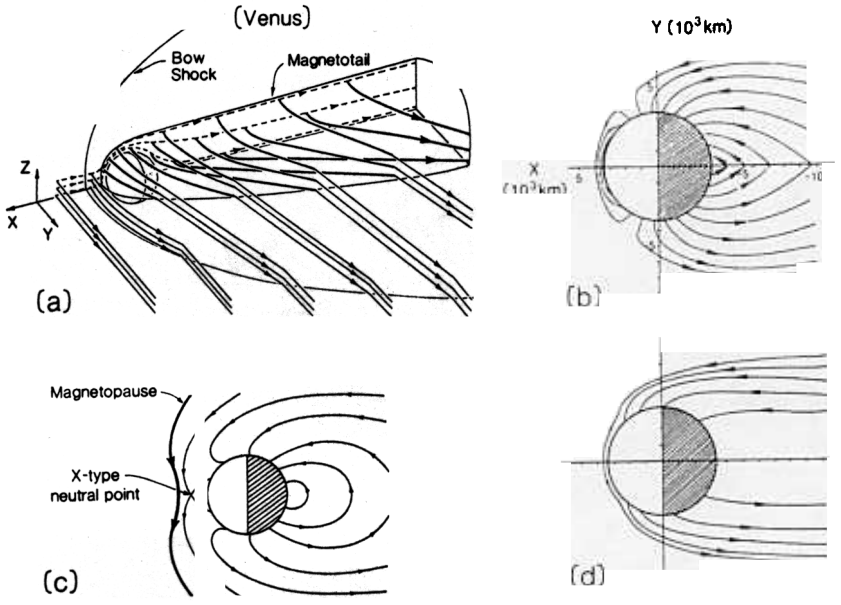

Fig. 15. The variety of possible configurations of the Martian magnetotail envisioned by various authors: (a) an "induced" magnetotail like that of Venus (from Saunders and Russell 1986; see also Vaisberg and Zeleny 1984); (b) a traditional Earth-like magnetotail; (c) a magnetotail wherein dayside magnetic merging plays a role (figure from Rassbach et al. 1974); and (d) a magnetotail that encompasses all of the flux leaving the day side of the planet so that a "bald" spot or band results.

problem like the bow-shock observations. On the other hand, except at the terminator, they are fairly consistent with the tail locations of the planetopause identified by the Phobos 2 investigators (Riedler et al. 1989; Rosenbauer et al. 1989*a*).

The plasma properties and magnetic field observed by the Phobos 2 spacecraft inside of the inferred obstacle boundary are especially valuable for investigating the question of an intrinsic magnetic field. In particular, the observations by Riedler et al. (1989*a*) of magnetotail lobe polarities that change with the orientation of the interplanetary magnetic field (also see Yeroghenko et al. 1990) suggest that any intrinsic field is too weak to have much effect at ~2.8 R_M downstream in the plane of the orbit of the natural satellite Phobos. These magnetic field observations, together with the absence of solar-wind protons, are very reminiscent of what has been observed behind Venus (see Saunders and Russell 1986; Mihalov and Barnes 1982). As comparisons with Venus are a key factor in the analysis of these observations, this is an appropriate point at which to begin the discussion of the Venus analogies.

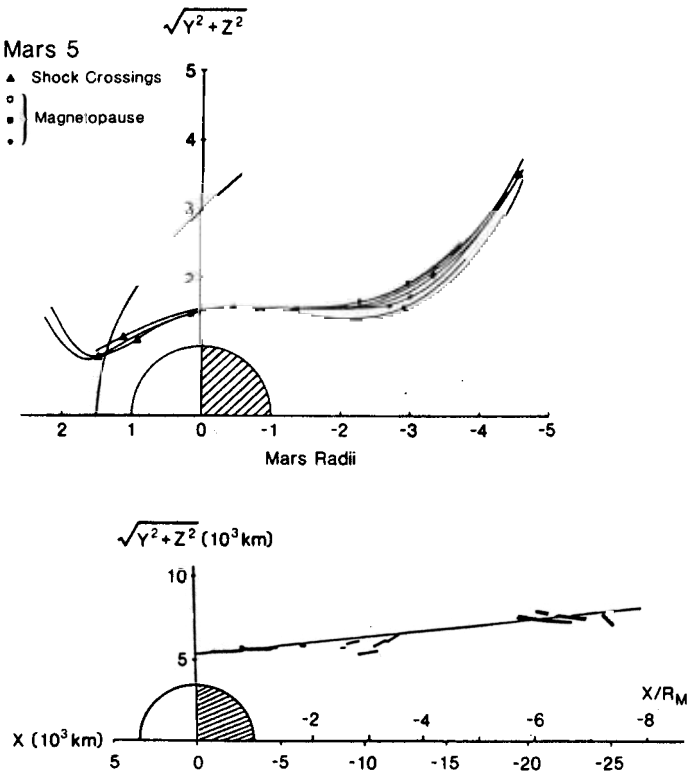

Fig. 16. The tail boundary at Mars inferred from Mars 2 and Mars 5 plasma measurements that show a change in flow and temperature characteristics at these locations (figure adapted from Vaisberg and Smirnov 1986).

F. Mars-Venus Comparisons

Although one should not jump to the conclusion that Mars is more like Venus than any other planet, there are compelling reasons for drawing analogies. For one, both are weakly magnetized obstacles to the solar wind that are little more than planet sized, as mentioned earlier. Both are terrestrial planets with some similarities in their surfaces and atmospheres, and they both reside in the inner solar system where the solar-radiation flux and the solar-wind density are substantial. Thus it is no surprise that comparative analyses of the Mars and Venus environments have proven illuminating. An assessment of our state of knowledge for Venus can be found in a review paper by Luhmann (1986). In this section, we return to the basic features of the solar-wind interaction considered earlier, but this time focus on the contrasts and similarities between our two neighboring planets.

1. Bow Shock. In their analysis of the bow-shock shape of Mars, Slavin and Holzer (1982) made the comparison with the bow shock of Venus after scaling to make the planetary radii equal. This comparison is included in Fig. 7, where it is seen that the Mars near-terminator bow shock determined from the Mars spacecraft data lies at about the same relative distance from the planet as the near-terminator shock at Venus at solar maximum, but well outside of the bow shock at Venus at solar minimum. As most of the Mars data used by these authors was from the approach to solar minimum, and as Venus at solar minimum is more Mars-like in its weakness of ionosphere pressure compared to solar-wind pressure, the result points to a difference in the two solar wind interactions. The recent observation by Phobos 2 of a near-solar-maximum terminator shock position of ~2.7 R_M (Schwingenschuh et al. 1990), well above the Venus solar maximum position, confirms this. The inferred Martian obstacle must be significantly more flared at the terminator than the obstacle at Venus under similar solar activity conditions. However, (at least for high solar activity at Venus) the bow shocks of both planets share the characteristic that their inferred dayside obstacle from gas-dynamic models is larger than the observed ionopause.

In another study, Slavin and Holzer (1981) presented data showing the dependence of the Mars bow shock radius in the terminator plane on incident solar-wind dynamic pressure, which they compared with the expected behavior for a purely dipole field obstacle in the solar wind. The size of a magnetic obstacle, and hence the bow shock, is expected to respond much more sensitively to solar-wind pressure than the size of a relatively incompressible ionospheric obstacle like Venus. Their display, which is shown in Fig. 17a, does not make a good case for dipole-field obstacle behavior. Rather, it suggests that although the bow shock position is quite variable, this variability is not clearly related to solar-wind dynamic pressure. An analogous plot for Venus, reproduced in Fig. 17b (cf. Luhmann et al. 1987), implied a like insensitivity of Venus' obstacle to the solar-wind dynamic pressure, thus pointing to a similarity between the planets that is in contrast to purely magnetospheric behavior.

Other aspects of the bow shock comparisons, such as a search for a Venus-like solar-cycle dependence of the Martian bow shock position (Alexander and Russell 1985), can now be considered because there are data for a wide range of solar activity. Figure 18 shows where the various missions to Mars have occurred with respect to the sunspot cycle. A comparison between the terminator bow-shock location observed during the Mars missions with that observed by Phobos 2 should give an indication of the effective Martian obstacle's variation with solar EUV radiation. As mentioned before, Schwingenschuh et al. (1990) report an average terminator bow-shock location for the near-solar-maximum conditions of Phobos 2 observations of ~2.7 R_M. The earlier results shown in Fig. 7 give a distance of ~2.4 R_M. A change of ~0.3 planetary radii was what was found at Venus where the terminator shock position moved from ~2.1 to ~2.4 planetary radii (Alexander and Russell 1985). So we are left with mixed results. On the one hand, the Mars

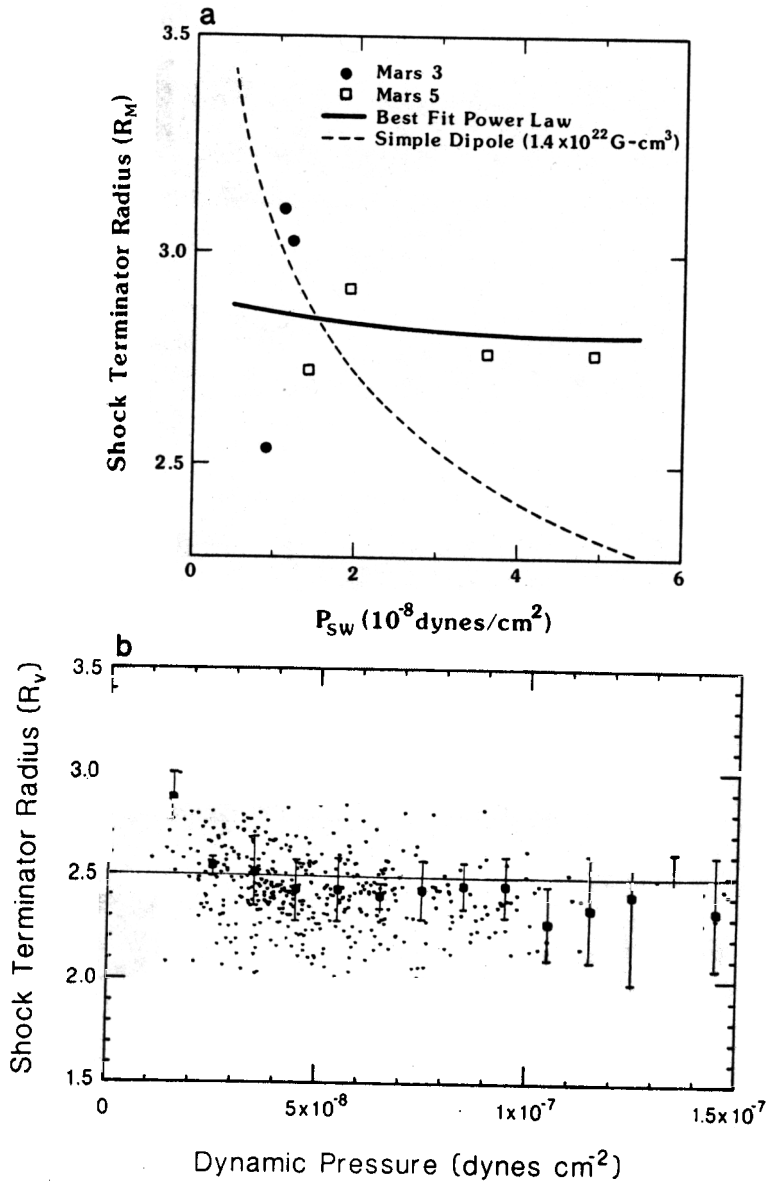

Fig. 17. (a) Radial distance of the observed Martian bow shock projected to the terminator plane vs solar-wind dynamic pressure. The dashed line shows the expected response for a weak dipole-field obstacle. The solid line describes the best fit of a low-order polynomial to the data (figure from Slavin et al. 1983). (b) Corresponding plot from Pioneer Venus Orbiter bow-shock observations that shows a similar insensitivity of the Venus obstacle to solar-wind pressure.

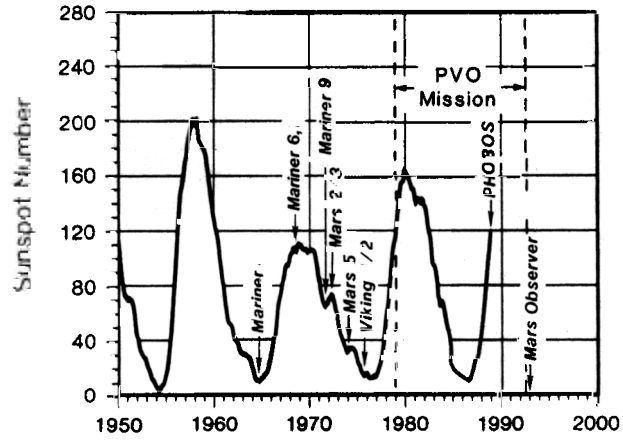

Fig. 18. A chronology of Mars missions referenced to the sunspot cycle. The period covered by the Pioneer Venus Orbiter (PVO) mission is indicated for comparison.

bow-shock insensitivity to the solar wind and its sensitivity to solar EUV argues that Mars is a Venus-like obstacle with negligible intrinsic magnetic field. On the other hand, the bow-shock position comparison raises the question of why the Martian bow shock and hence obstacle boundary are relatively farther from the planet than they are at Venus. Nevertheless, we have gained insight as to the differences that must be explained. One possibility is that the Martian atmosphere has a sufficiently different dependence on altitude and solar zenith angle that the effective obstacle is in fact a different shape (e.g., see Zhang et al. 1990*b*). An alternative explanation is that there are plasma physical processes at work in the solar-wind interaction with Mars (e.g., the finite gyroradius effects mentioned earlier, or charge exchange between solar wind protons and exospheric hydrogen atoms) that modify the magnetosheath in ways that are not as important at Venus; and of course there is the possibility that magnetic fields of either internal or induced origin are determining the different obstacle shape for Mars. The weight of evidence from further observations or analyses is needed to select from among these or other options.

2. Magnetosheath. The Russell et al. (1984) comparison of the Martian magnetosheath magnetic field with the gas-dynamic model discussed earlier had also been carried out for many cases of Pioneer Venus observations of the Venus magnetosheath with similarly good agreement (see Luhmann et al. 1986*b*). Vaisberg et al. (1976*a*,*b*) presented the plasma measurements along the Mars 5 spacecraft orbit in a form that demonstrated an analogous favorable comparison of some model and observed plasma properties (see Fig. 10), as was done for Venus by Spreiter and Stahara (1980) and Mihalov and Barnes (1982). Thus it seems safe to say that, for both planets, the gen-

eral features of the magnetosheaths are understood. An understanding of the details, including the formation and properties of a magnetic barrier at the inner boundary, and the effects of the picked-up planetary ions, awaits more sophisticated observational analyses (e.g., of the Phobos 2 data) combined with sophisticated global models. For example, it is known that both planets have extensive oxygen exospheres (Nagy and Cravens 1988). Phillips et al. (1987) found evidence that the magnetosheath magnetic-field strength and draping at Venus are enhanced on the side of the magnetosheath where most of the associated asymmetrically picked-up ions should be found. This evidence was detectable only because of the extensive spatial and temporal coverage provided by the Pioneer Venus Orbiter database, which still has no equal at Mars.

Planetary pick-up ions, probably O^+, have also been detected in the Venus magnetosheath around the terminator (Mihalov and Barnes 1981; Phillips et al. 1987; Intriligator 1989) and downstream (Mihalov and Barnes 1982). Together with the aforementioned heavy-ion observations at Mars (Vaisberg and Smirnov 1986; Lundin et al. 1989; Rosenbauer et al. 1989; Lundin et al. 1990*a*,*b*) and the observation that the bow shocks of both Mars and Venus require a larger obstacle than the ionosphere to explain their shapes, these observations suggest that a magnetic field and heavy ion mantle in the inner magnetosheath may be the effective obstacle to the solar wind at both planets. (See Wallis [1982] for a discussion of pick-up ion effects at Venus, and Wallis and Ip [1982] for additional discussion of the comparison with Mars.) The mixture of solar wind and ionospheric electrons observed in the mantle regions of both planets (Spenner et al. 1980; Shutte et al. 1989; Nagy et al. 1990) indicate that at least solar-wind electrons find the boundary of this obstacle permeable.

Earlier, we alluded to the observation that the draped magnetosheath field becomes disturbed by convected fluctuations when the subsolar bow shock is quasiparallel. This effect was easily seen at Venus where the magnetic field throughout the magnetosheath became highly variable on such occasions (see Luhmann et al. 1983). Quasiparallel subsolar bow shocks may also be responsible for some of the observed field fluctuations in the Martian magnetosheath (see e.g., Dolginov 1976; Riedler et al. 1989*a*). However, since the proton gyroradius scale is much more important at Mars, there may also be additional sources of plasma instability that contribute to the local waves and turbulence.

3. Ionosphere. Although the ionospheres of Venus and Mars have been individually observed and modeled, their common features have been compared in only a few reviews without any particular emphasis on analogies (see e.g., Schunk and Nagy 1980; Mahajan and Kar 1988). Yet, both ionospheres exhibit the distinguishing features of O_2^+ compositional domination at altitudes below ~200 km (see Fig. 9 of chapter 30), H^+ and O^+ domination above 200 km, and ion and electron temperatures that increase with altitude far more rapidly than those that would result from heating by solar radiation alone (see Fig. 11 of chapter 30).

As discussed earlier, after the Viking Lander results became available, several investigators (Chen et al. 1978; Rohrbaugh et al. 1979; Johnson 1978) attempted to explain the observed temperature profiles using a combination of uniform, near-horizontal magnetic fields and topside and local heating. Cravens et al. (1979,1980) performed nearly the same analyses for the temperatures in the Venus ionosphere as measured on the Pioneer Venus Orbiter. As a whole, these studies demonstrated that with some additional heating and magnetic field, one can approximate the observations, but there is considerable ambiguity as to the appropriate combination of heating and magnetic field. Nevertheless, the necessity of similar modifications to the ionospheric models for both planets make the Venus *in situ* observations of the ionospheric magnetic field particularly relevant.

Specific comparisons of the Venus and Mars ionospheric properties have been discussed by Luhmann et al. (1987). These authors took into account the fact that, during the low-altitude phase of the Pioneer Venus Orbiter mission (when solar maximum conditions prevailed), Venus should be most like Mars on the few occasions when the solar-wind dynamic pressure at Venus exceeded the maximum thermal pressure in the ionosphere (see Fig. 5). The Venus ionosphere properties under these conditions are illustrated, together with the corresponding Viking Lander data from Hanson et al. (1977), in Fig. 19. Both ionospheres exhibit comparably steep ion-temperature gradients (see Fig. 19a), and the lack of a well-defined ionopause cutoff in the density profile (see Fig. 19b), but the most important aspect of this comparison is the contemporaneous behavior of the magnetic field at Venus. The induced horizontal ionospheric magnetic field was found to increase in magnitude, up to ~150 nT, as necessary to produce pressure balance with the incident solar wind. Luhmann et al. (1987) suggested that the weak Martian ionosphere could stand off the solar wind in the same way. In fact, only a few 10s of nT of ionospheric field would perform this function on a typical day on Mars. The magnetic field needed to explain the Viking temperature measurements would be a natural part of such a scenario. Mars-like conditions may in fact be the norm during solar minimum at Venus when the ionospheric thermal pressure is expected to be low compared to the solar-wind pressure (Knudsen et al. 1987; Luhmann et al. 1990). Although there are no *in situ* ionospheric data for Venus at solar minimum, the comparison in Fig. 20 of radio-occultation profiles obtained from Mars and from Venus at solar minimum, showing a like absence of a distinct ionopause on their topsides (also see Luhmann et al. 1990; Zhang et al. 1990*b*), supports this idea. Shinagawa and Cravens (1989) have now adapted a magnetohydrodynamic model of the magnetization of the ionosphere of Venus to Mars with this analogy in mind. Of course, on occasions when the solar-wind dynamic pressure is extraordinarily

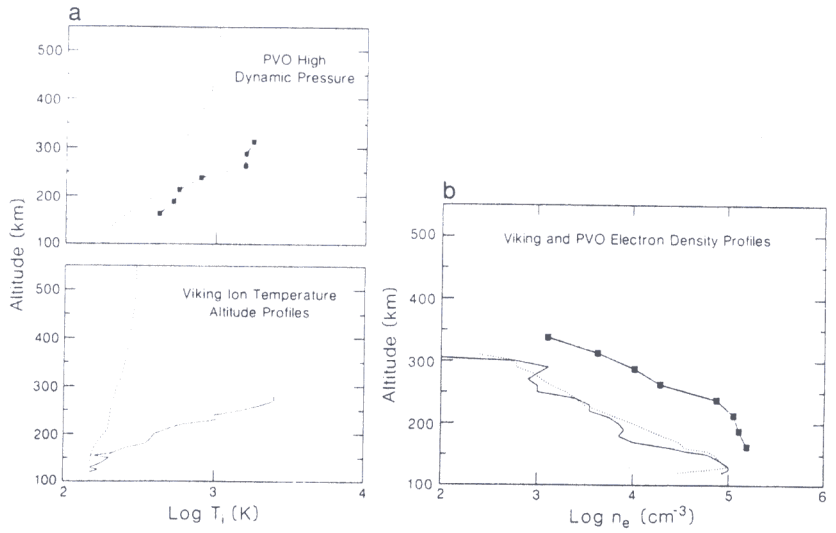

Fig. 19. (a) (bottom) Comparison of ion temperature profiles observed in the Martian ionosphere by the Viking Landers (Hanson et al. 1977) and (top) at Venus by Pioneer Venus Orbiter (PVO) when the solar-wind pressure was high compared to the ionospheric thermal pressure as at Mars. The dashed lines show the profiles expected for solar radiation heating alone. (b) Comparison of electron-density profiles from the same data sets (figure from Luhmann et al. 1987). In both (a) and (b) the black squares represent medians of PVO data. The data from the Viking Landers are shown by solid and dotted lines.

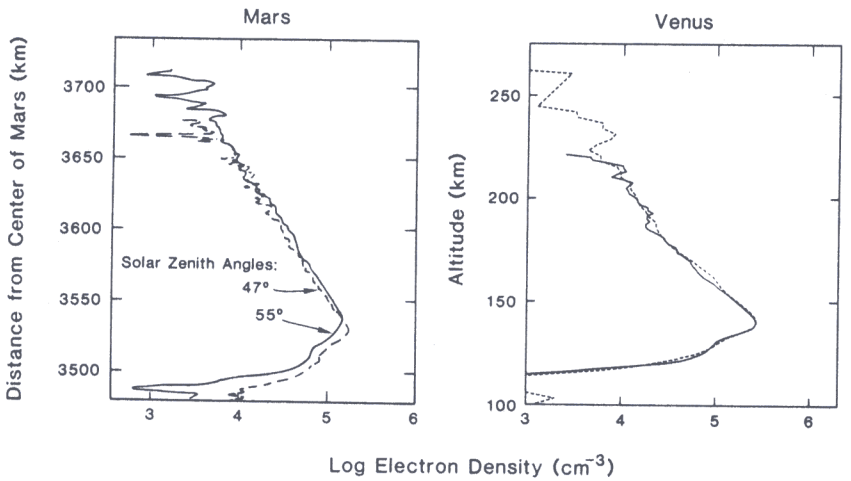

Fig. 20. Examples of radio-occultation profiles obtained at Mars and for the day side of Venus during solar minimum. The Mars data are from Mariner 9 and the Venus data are from Pioneer Venus Orbiter (figure adapted from Kliore et al. 1972).

low, or the solar EUV flux is extraordinarily high (e.g., at solar maximum), Martian ionospheric thermal pressure alone might be sufficient to stand off the solar wind in a Venus-like manner. However, only extensive *in situ* or radio-occultation measurements of the ionosphere with supporting solar-wind measurements would allow us to witness and prove such occurrences at Mars.

Another feature of the ionosphere of Venus that corresponds to conditions at Mars is the occasional depletion of nightside ionization. Radio-occultation observations at Mars show that the nightside ionosphere is generally rarefied although variable (e.g., see Breus and Gringauz 1980). Venus is known to have a substantial nightside upper ionosphere at solar maximum when dayside ionization is transported freely to the night side by pressure gradient forces (Knudsen et al. 1980). However, when the solar-wind dynamic pressure is high, or Mars-like conditions prevail, the nightward ion flow is choked off because the terminator ionopause altitude is low. On these occasions, the nightside ionosphere is confined to the region below ~200 km where the source is thought to be particle precipitation. At these times, Venus is said to have a disappearing ionosphere on the night side because the *in situ* data, from altitudes above ~150 km, show only weak, highly variable densities (see Cravens et al. 1982). According to the Venus *in situ* and radio-occultation experiment results, this condition also seems to prevail during solar minimum, when the dayside ionosphere is always weak compared to the solar-wind pressure (Knudsen et al. 1987; Knudsen 1988). For the same reason, the nightside ionosphere of Mars may always be "disappearing," or absent, except when the solar-wind pressure is extraordinarily low or the solar EUV flux is extraordinarily high (see, e.g., Zhang et al. 1990*a*). Of course, this interpretation assumes that the particle precipitation source at Mars is weak. While the more rapid rotation of Mars should have a small effect on the nightside ion densities, recombination is so rapid that it is expected to be minor.

It is worth noting that prior to the Pioneer Venus Orbiter *in situ* mission, when most of the Mars data were being interpreted, we did not know about the behavior of ionospheric magnetic fields at weakly magnetized planets; we did not know about "disappearing" ionospheres; and we did not know in general how ionospheric obstacles to the solar wind respond to excessive solar-wind pressures. The observations at Venus have allowed us to assess the Mars observations from an informed perspective (e.g., see Zhang et al. 1990*a*,*b*).

4. Wake and Tail. From the terrestrial example, we know that the wake of a magnetized planet is a region of low-density plasma dominated by magnetic fields with a large sunward or antisunward component. These fields have a fixed polarity consistent with the permanent magnetic field of the

planet. A hot plasma sheet separates the regions of opposite magnetic polarity, which are referred to as tail lobes. In contrast, we know from the Venusian example that an induced magnetotail has a magnetic field with a similar structure consisting of two lobes of sunward or antisunward fields, but in this case the polarity is controlled by the orientation of the transverse component of the interplanetary magnetic field (e.g., see Fig. 15). Moreover, while the tail of Venus has an associated solar-wind plasma "void" like the tail of a magnetosphere (Milahov and Barnes 1982), it may also have a boundary layer and possibly a plasma sheet of cold, heavy, presumably ionospheric ions. Vaisberg and Smirnov (1986) discussed the *in situ* measurements of the plasma in the vicinity of the Martian wake from the viewpoint of comparisons with Venus. On the one hand, these authors stress the similarities in the plasma behavior at Mars and Venus, with particular reference to the boundary layer of possibly heavy, low-energy ions observed at the transition between the solar wind and the tail cavity at both planets. On the other hand, they point out that the boundary shape from the plasma measurements, shown in Fig. 16, is quite different from that at Venus, with the terminator radius of the Martian tail of $\sim 1.5\ R_M$ significantly greater than the Venus tail terminator radius of only ~ 1.2 planetary radii. This difference is supported by the Phobos 2 observations (Riedler et al. 1989; Rosenbauer et al. 1989).

The question of the magnetic field behavior inside the tail boundary at Mars compared to that at Venus was difficult to examine prior to the Phobos 2 mission because we did not have adequate deep-tail data for Mars. At Venus, such a database provided unambiguous evidence that the polarity of the field is controlled by the orientation of the interplanetary magnetic field (Saunders and Russell 1986). Vaisberg and Smirnov (1986) considered that what was observed around the tail boundary from the Mars spacecraft was sometimes influenced by the direction of the interplanetary field, as reported for Venus, but sometimes behaved independently. These authors suggested that a compromise was in order to explain the tail observations. They proposed that the tail field configuration may be some hybrid combination of intrinsic field emanating from the poles of a weak dipole and Venus-like draped interplanetary field supplying the field in the neighborhood of the magnetic equator. We are now more constrained by observations, which show that the magnetotail at the orbit of the natural satellite Phobos (at $\sim 2.8\ R_M$) and beyond is "induced" like that of Venus (Riedler et al. 1989; Yeroshenko et al. 1990). However, because of the lack of measurements in the polar regions of the magnetotail, one still cannot rule out the hybrid-tail possibility for Mars.

G. Mars-Earth Comparisons

1. Bow Shock. The shape of the Martian obstacle as inferred from the bow-shock shape is more flared than the corresponding obstacle at Venus,

and is in fact more consistent with the shape of a magnetopause like that of the Earth. However, the contrast between the sizes of the two bow shocks, as illustrated by Fig. 21, is striking. Slavin and Holzer (1981) included Venus in this figure for the purpose of emphasizing the comparison of the Martian bow shock with those of known atmospheric and magnetospheric obstacles. Because the bow shocks of Mars and Venus are both much closer to the planet than that of Earth, and much smaller in absolute scale, finite solar-wind proton gyroradius effects and planetary ion pick-up effects may produce distinctive shock structure not found at the terrestrial bow shock (e.g., see Moses et al. 1988), although such features have not yet been identified at Venus.

2. Magnetosheath. As was discussed earlier, one of the consequences of a quasiparallel subsolar bow shock at Venus is that the magnetosheath is filled with convected turbulent magnetic fields. A similar effect of the quasi-

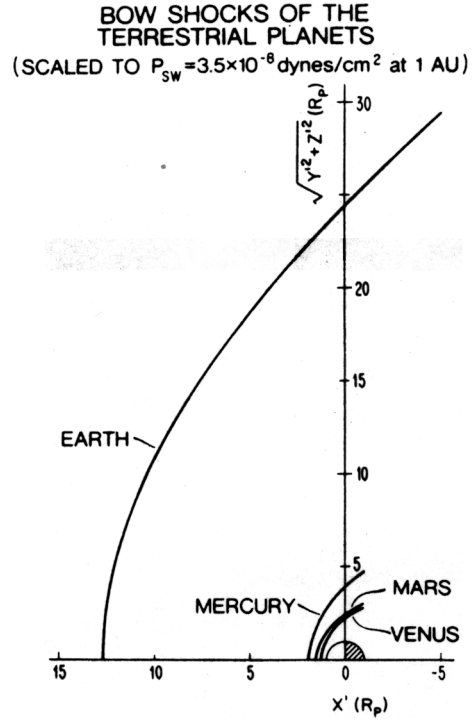

Fig. 21. Comparison of bow-shock sizes at the terrestrial planets. The bow shock positions were scaled to a common solar-wind dynamic pressure of 3.5×10^{-8} dyne cm^{-2} (figure from Slavin and Holzer 1981).

parallel shock on magnetosheath fields is observed at Earth (see Luhmann et al. 1986*b*), but the scale of the turbulent fluctuations relative to the subsolar magnetosheath thickness and the obstacle is much smaller. In addition, the distance for attenuation of the turbulent fields between the bow shock and the obstacle is much greater at Earth. Thus Mars is in this sense less like Earth than like Venus. However, it is worth repeating here that the large-scale magnetosheath fields for all of these obstacles appear to be at least roughly consistent with the gas-dynamic models of field draping.

3. Ionosphere. If Mars had a significant intrinsic dipole field, the ionosphere of Mars should be similar to that of Earth in at least one respect. Both planets have short rotation periods (~24 hr) that would, as at Earth, produce a particular diurnal asymmetry in the ionosphere. The electron density at middle latitudes at the Earth does not decay rapidly after sunset because of the large reservoir of mainly hydrogen ions that are stored in the overlying plasmasphere. This dipolar magnetic field reservoir is refilled during the daytime by upward ion flow and partially depleted at night by downward ion flow that helps to maintain the nightside ionosphere, especially near dusk, against the loss of ions by recombination at low altitudes (see Schunk and Nagy 1980).

An intrinsic magnetic field at Mars could either inhibit or promote the formation of a nightside ionosphere, depending upon its strength. An intrinsic field that is at a large angle to the nominal plasma velocity should inhibit the horizontal transport of ions from the day side, thus preventing the formation of a dense nightside upper ionosphere sensitive to incident solar-wind dynamic pressure like that of Venus at solar maximum (see Knudsen et al. 1980). On the other hand, if the magnetic field strength was large enough, an Earth-like plasmasphere should form, creating a reservoir large enough to maintain an ionosphere well after sunset. Thus the detection of dawn/dusk asymmetries in the nightside ionosphere could provide clues to the existence of a substantial intrinsic magnetic field. The available radio-occultation data of the nightside ionosphere have not yet been used to investigate these possibilities. However, they do tell us that the nightside ionospheric density is somewhat lower at Mars than at Venus (see Lindal et al. 1979; Knudsen et al. 1987). Although this suggests the possibility of a dipole field that is too weak to form a significant plasmasphere but strong enough to inhibit nightward flow, we know that at Mars ionosphere conditions are more like Venus at solar minimum where the nightward flow is effectively shut-off by the low terminator ionopause (Knudsen 1988). The weakness of the Martian nightside ionosphere is thus, by itself, inconclusive.

4. Wake and Tail. Some experimenters (notably Gringauz et al. 1976) considered that the plasma properties observed by the Mars spacecraft at the

edge of the Martian tail resembled the plasma in the terrestrial plasma sheet, which fills the closed high-latitude dipole field lines that stretch out into the terrestrial magnetotail. Others (Vaisberg 1976; Vaisberg and Smirnov 1986) argued strongly for a Venus-like boundary layer interpretation. But, as discussed previously, the key to establishing the presence of an intrinsic magnetotail with its fixed polarity field anchored to the planet lies in central wake magnetic-field measurements.

Dolginov (1976) believed that Mars spacecraft magnetic measurements near the edge of the Martian tail showed evidence for behavior that was independent of the interplanetary field orientation. However, his analyses were based on the comparison of x or radial (sunward/antisunward) components of the field upstream near the tail boundary. Because an induced tail consists of the draped *transverse* or perpendicular (to the flow) component of the interplanetary field (see Fig. 15), an argument based on the radial component is not really valid (Vaisberg and Smirnov 1986). The interpretation of Dolginov also did not allow for rotations of the perpendicular component of the interplanetary field which can create a layered structure of sequentially draped fields. After Phobos 2, we know that at least the magnetic properties of the Martian tail near the orbit of Phobos are more like those of Venus than those of Earth (Yeroshenko et al. 1990). Nevertheless, Vaisberg and Smirnov (1986) found grounds for arguing in favor of at least some Earth-like intrinsic magnetotail contribution to the Martian tail because it could explain the greater cross section of the Mars obstacle at the terminator relative to that at Venus. Likewise, some of the Phobos 2 plasma investigators consider that there are Earth analogies to the ion "beams" seen in the Martian tail (see Lundin et al. 1989).

IV. SOLAR-WIND INTERACTION WITH PHOBOS AND DEIMOS

The natural satellites of Mars, Phobos and Deimos, are discussed at length in chapters 36, 37 and 38. They are much like the other minor bodies in the solar system in that they appear to be small, irregular, atmosphereless fragments of some larger body. These bodies orbit Mars near its equatorial plane at ~2.8 planetary radii and ~7 planetary radii, respectively. In these orbits, Phobos and Deimos regularly traverse the upstream solar wind, move through the Martian magnetosheath, and cross the wake and tail region. Their interaction with, and influence on, the plasma environment of Mars is probably not important for our basic understanding of the Martian magnetic field and solar-wind interaction, but it nonetheless is of intrinsic interest in our effort to become knowledgeable about the Mars system as a whole.

The interaction of a flowing plasma with Phobos and Deimos should be similar to that of asteroids in the solar wind, a subject on which little work has been done. The Moon is the closest prototype for which there exists both

observations and theories. In particular, Spreiter et al. (1969) formulated a gas-dynamic model for the solar-wind interaction with a spherical nonconducting body, with no atmosphere, that absorbed the incident solar-wind plasma. The characteristics of that interaction were the absence of a shock wave in front of the body, and a wake void in the solar-wind plasma with a boundary in which the interplanetary magnetic field was perturbed after appearing to pass freely through the body. What limits the applicability of this picture to Phobos and Deimos are the sizes of these bodies compared to the Moon. All are much larger than the ~10 m Debye length of the solar-wind plasma, a condition under which the plasma can be treated as a fluid as in gas-dynamic theory. However, the proton gyroradius of ~600 km in the solar wind, which is much larger than Phobos or Deimos with their diameters of ~22 km and ~13 km, respectively, is such that the particle nature of the solar-wind plasma must be considered in a description of their interactions. As far as the environment of Mars is concerned, one can speculate that these bodies are so small compared to the gyroradii of solar-wind ions that their ion wakes are minimal and hence their perturbing effect on the plasma around Mars is negligible.

In spite of this assessment, it should be mentioned that at least one author (Bogdanov 1981) believed that the Mars 3 spacecraft detected evidence of an unexpectedly strong perturbation of the solar wind by Deimos. His explanation for the strength of the interaction was that Deimos was outgassing and that the emitted particles were producing the perturbation. There has been no other evidence for strong outgassing activity on Deimos or on Phobos, although the Phobos 2 investigators detected electric and magnetic-field perturbations when the spacecraft crossed the orbit of Phobos at a considerable distance from the satellite (Riedler et al. 1989*a*; Grard et al. 1989; Dubinin et al. 1990). It is certainly possible that these bodies are a source of atoms, ions and possibly dust in the Martian environment. Atoms and ions could result from the sputtering of their surfaces by energetic solar particles and Martian exospheric pick-up ions, while dust could conceivably be produced by micrometeoroid impact (see, e.g., Ip and Banaszkiewicz 1990). The ions should be carried away by the solar wind in the same manner as the exospheric ions, while the atoms produce a neutral torus around Mars (see Ip 1988). The smaller (submicron) dust particles would undergo quite complicated motions because they are subject to both gravitational forces and electromagnetic forces as they become charged in the Martian plasma environment (Horanyi et al. 1990), while larger particles would remain in the orbit of the satellite, forming a "ring." The latter could, in principle, produce the field perturbations observed on Phobos 2, but these ideas remain to be tested in light of the negative dust ring search using Viking data (Duxbury and Ocampo 1988).

V. CONCLUDING DISCUSSION

A. Summary of our Current Understanding

Estimates of the magnetic field of Mars from its solar-wind interaction have experienced a fairly consistent history as indicated by Fig. 8. However, at the time of writing this review we know with certainty only the following facts relating to the Martian field and solar-wind interaction:

1. The bow shock and magnetosheath of Mars indicate the presence of an obstacle to the solar wind that is somewhat larger than the size of the planet and its observed ionosphere, and also relatively larger than the Venus obstacle under comparable conditions.
2. The intrinsic magnetic field of Mars must be no greater than 1.5×10^{12} T m^{-3} or $\sim 10^{-4}$ times as strong as that of Earth (whose dipole moment is $\sim 8 \times 10^{15}$ T m^{-3}) to produce an obstacle of such small size.
3. At least for solar minimum conditions, like those prevailing at the time of the Viking Landers, the ionospheric plasma (thermal) pressure is insufficient to balance the incident solar-wind pressure by itself.
4. The ion and electron temperatures in the Martian ionosphere indicate the presence of local horizontal magnetic fields and heat sources in excess of solar radiation alone.
5. The plasma and field properties observed around Mars resemble those observed around Venus. In particular, planetary O^+ ions scavenged by the solar wind have been detected at both planets.
6. The magnetic field in the equatorial wake of Mars, at radial distances at and beyond the orbit of Phobos (~2.8 R_M) appears to be of predominantly interplanetary origin like that in the induced magnetotail of Venus.

The rest is speculation and inference. Using well-probed Venus as a model, one can find analogies that lead one to conclude that the two planets are much alike with their mutually weak intrinsic fields and atmospheric obstacles to the solar wind. From the observations in hand, it is easy to say that Mars probably has a Venus-like ionospheric magnetic field to help it stand off the solar wind, but we cannot know that this is true until we further probe the regions of space inside the dayside Martian obstacle boundary. Similarly, we do not know whether there is a field of planetary origin in the low-altitude wake. At this point, one cannot rule out the possibility that there is an intrinsic Martian dipole field of marginal importance that is responsible for the differences between Mars and Venus that we observe—in other words, that Mars is a "hybrid" obstacle.

B. Future Prospects

At the time of this writing, we are fortunate to be on the threshold of a new era of Mars exploration. The Soviet Phobos 2 spacecraft arrived at Mars

in January of 1989. It carried instruments capable of measuring the plasma and field environments of both Mars and Phobos. Even though the mission came to a premature end, the magnetic field experiment has given us an unprecedented database from which to extract information on the sensitivity of the deep tail field polarities to interplanetary conditions. As shown by Fig. 18, Phobos 2 provided the first measurements of the Martian space environment near the maximum phase of the solar cycle. Phobos 2 also carried sophisticated experiments capable of measuring picked-up planetary ions over a broad energy range, thus leading to empirical estimates of the importance of solar-wind scavenging for atmosphere evolution and giving information about the local energetic particle environment. The U. S. Mars Observer spacecraft, scheduled for launch in 1992, will obtain a large magnetic field database, although the circular ~350 km polar orbit is not well suited for measurements free from the interference of the complex near-planet plasma environment. (At Venus, tail "rays" of ionospheric plasma and complicated magnetic-field structures associated with the solar-wind interaction were observed in the low altitude wake [see Brace et al. 1987].) Nevertheless, Mars Observer will be the lowest altitude probe to carry a magnetic-field experiment with the possible exception of the Soviet Mars 94 spacecraft. The latter is planned to provide aeronomy and particles and fields observations along an elliptical orbit that will probe Mars space to altitudes lower than the Mars Observer orbit.

Thus, plans are underway for a next salvo of Mars spacecraft to further define the upper atmosphere and space environment of Mars. The U.S. Mars Aeronomy Orbiter (described in NASA Tech Memo 89202, JPL, October, 1986) has yet to gain approval, but it now has an additional important application as a precursor mission to human landings in the possible future space exploration initiative. Together, these missions will replicate, and improve upon, the mission to Venus undertaken by the Pioneer Venus Orbiter. If these plans proceed as anticipated, many of the outstanding questions in this chapter can be answered within the decade.